Fundamental Research xxx (xxxx) xxx

Contents lists available at ScienceDirect

Fundamental Research

journal homepage: http://www.keaipublishing.com/en/journals/fundamental-research/

Article

Copper-doped CeZn catalysts for efficient CO_2-assisted oxidative dehydrogenation of propane: Mechanistic insights and performance optimization

Cedric Karel Fonzeu Monguen [a,b], Samuel Daniel [a,c], Ling-Nan Wu [a,d], Hannington Nevin Otieno [a,c], Patrick Lott [b], Wu Qin [e], Olaf Deutschmann [b], Zhen-Yu Tian [a,c,*]

[a] Institute of Engineering Thermophysics, Chinese Academy of Sciences, Beijing 100190, China
[b] Institute for Chemical Technology and Polymer Chemistry, Karlsruhe Institute of Technology (KIT), Engesserstr. 20, Karlsruhe 76131, Germany
[c] College of Engineering, University of Chinese Academy of Sciences, Beijing 100049, China
[d] State Key Laboratory of Coal Conversion, Institute of Engineering Thermophysics, Chinese Academy of Sciences, Beijing 100190, China
[e] School of New Energy, North China Electric Power University, Beijing 102206, China

ARTICLE INFO

Article history:
Received 28 March 2025
Received in revised form 29 October 2025
Accepted 10 November 2025
Available online xxx

Keywords:
Cu(Ce/Zn)
CO_2-ODHP
Lattice oxygen
Stability
Cu loading
CO_2 activation

ABSTRACT

The use of CO_2 as a mild oxidant for the oxidative dehydrogenation of propane (CO_2-ODHP) is crucial for achieving net-zero carbon emissions and mitigating greenhouse gases that contribute to global warming. In this study, a CeZn catalyst was synthesized using the wet impregnation method and applied for CO_2-ODHP. Incorporating Cu into the (CeZn) lattice enhanced both propane conversion and yield by leveraging the redox properties of (CeZn) to activate CO_2 into CO and O*, which facilitated the cleavage of propane C–H bonds. Characterization of the catalyst's physicochemical properties revealed that doping Cu into (Ce/Zn) significantly increased the specific surface area and pore volume due to the presence of Cu^{2+} species, promoting the mobility of lattice oxygen (O_{Lat}), and thereby improving C_3H_8 conversion. Additionally, the transfer of oxygen from Ce^{4+} to Ce^{3+} during the reaction contributed to the highest propene selectivity observed for the copper-free catalyst. The catalytic activity was maintained even after several hours of propane conversion at 550 °C. All catalysts demonstrated relatively stable performance, with the highest and lowest relative deactivation rates of < 6 % and 4 %, respectively, observed in 0 %Cu(Ce/Zn) and 3 %Cu(Ce/Zn). DFT calculations revealed that the CuO-ZnO cluster on the CeO_2 (111) surface effectively promotes the activation of CO_2. Thus, modifying (Ce/Zn) with Cu is a promising strategy for enhancing propene yield in CO_2-ODHP.

1. Introduction

Propene (C_3H_6) is a vital starting point material for the production of acrylic acid, polypropylene, acrolein, and polyacrylonitrile [1]. It is synthesized through several methods, including the naphtha steam-cracking process, fluid catalytic petroleum cracking, and direct dehydrogenation of propane (DHP) [2]. Due to the growing market demand for propene and the shortage of petroleum resources, its production has received significant attention in the past few years [3]. However, the endothermic DHP is an energy-intensive process, which can lead to coke deposition on the catalyst's surface [4]. To address this issue, molecular oxygen (O_2) has been utilized, as it activates at a low reaction temperature and effectively removes coke. Despite the benefits of employing O_2 as an oxidant, the oxidative dehydrogenation of propane (ODHP) method tends to result in the total oxidation of propane (C_3H_8) to carbon dioxide (CO_2), contributing to a notable decrease in propene selectivity at high propane conversion rates [4]. This has led to the exploration of milder oxidants such as sulfur dioxide (SO_2), nitrous oxide (N_2O), and CO_2 as an alternative to O_2. These mild oxidants impede over-oxidation and only marginally restore metal oxide catalysts to their oxidative states [5]. Among these, CO_2 is particularly advantageous because it is less toxic than SO_2 and exhibits a high thermal capacity. Using CO_2 can also aid in carbon application, potentially reducing the propagation of greenhouse gases [6]. Additionally, CO_2 can help remove surface-adsorbed hydrogen (H_2) produced during DHP, thereby accelerating the dehydrogenation process and improving propane conversion [7]. Despite being a waste element and a greenhouse gas, the use of CO_2 has gained significant interest. However, activating CO_2 poses challenges due to its thermodynamic stability ($\Delta H_{298K}\circ = +164 kJ/mol$) [8]. Thus, developing an effective cat-

* Corresponding author.
E-mail address: tianzhenyu@iet.cn (Z.-Y. Tian).

https://doi.org/10.1016/j.fmre.2025.11.006

alyst for converting CO_2 in ODHP (CO_2-ODHP) to propene is highly desirable.

Among the numerous catalysts used for ODHP, zinc oxide (ZnO_x) has proven its potential in CO_2-ODHP for its amphoteric character, which moderates the overall surface acidity and improves structural stability [9]. Specifically, ZnO_x-based catalysts exhibited high catalytic activity for both DHP and CO_2-ODHP [10]. In Zn-based catalysts, the utilization of CO_2 helps to remove surface-adsorbed hydrogen, replenishing the active Zn^{2+} sites [9]. Recently, Ce-based catalysts have garnered interest for CO_2-ODHP because ceria (CeO_2) has a moderate basicity and excellent redox properties, facilitating the direct breakage of the C=O bond in the activation of CO_2 and providing abundant lattice oxygen for propane reaction and coke removal [11]. Additionally, Valenzuela et al. [12] revealed that the electron state transition from Ce^{4+} to Ce^{3+} represents the active stage for CO_2 activation to CO and O^* over Ce-based catalysts for ethane oxidative dehydrogenation. Thus, the interaction between Ce and Zn could enhance ODHP with CO_2. Furthermore, Cu has been shown to be very active at low temperatures during catalytic oxidation due to its known C-H activation ability, although with mild acidity [13], and recent findings indicate that the interplay between Cu and Cr has significantly improved the low-temperature ODHP [14]. Therefore, doping Cu into the (Ce/Zn) lattice could benefit the CO_2-ODHP. However, to date, the optimal loading of copper into the (Ce/Zn) support that might perform the dual function of activating CO_2 and controlling C-C breakage in ODHP for high-yield propene has yet to be established. Hence, it is essential to determine an adequate loading of Cu in the (Ce/Zn) structure that can selectively promote propene yield and induce CO_2 activation for ODHP.

In this study, various loadings of copper oxide were supported on (Ce/Zn) through impregnation methods and tested for CO_2-ODHP in a fixed-bed reactor. A comprehensive investigation on differences in the structure-activity dualism, as well as on the interaction between Cu, Ce, and Zn were conducted using techniques such as X-ray powder diffraction (XRD), Raman spectroscopy, N_2-physisorption, transmission electron microscopy (TEM), X-ray photoelectron spectroscopy (XPS), temperature-programmed reduction using H_2 (H_2-TPR), thermogravimetric analysis (TGA) and ultraviolet-visible spectroscopy (UV-vis). The findings obtained provide insights into the optimal loading of copper on (Ce/Zn) as an effective catalyst for CO_2-ODHP.

2. Experimental methods

2.1. Chemicals

Cerium nitrate hexahydrate ($Ce(NO_3)_3{\bullet}6H_2O$, 99.9 %), zinc nitrate hexahydrate ($Zn(NO_3)_2{\bullet}6H_2O$, 98 %), and copper II acetylacetonate ($Cu(acac)_2$, 98.5 %), all obtained from Sinopharm Chemical Reagent Co., Ltd., served as the precursors and were directly employed without any additional purification.

2.2. Catalyst synthesis

To prepare 1 %Cu (Ce/Zn), the equivalent weight of 1 wt.%Cu in $Cu(acac)_2$ was calculated (0.4 g $Cu(acac)_2$) and dissolved in 100.0 mL of ethanol. Then, 5.0 g of Ce $(NO_3)_3{\bullet}6H_2O$ and 5.0 g of Zn $(NO_3)_2{\bullet}6H_2O$ were added to the copper solution while stirring at a temperature of 60 °C for 3 h. The impregnated sample was then oven-dried at 100 °C for 12 h, followed by calcination in a furnace at 600 °C for 5 h, heating/cooling rate: 5 °C min^{-1}. Subsequently, 2 %Cu(Ce/Zn), and 3 %Cu(Ce/Zn) were prepared accordingly using 0.8 g $Cu(acac)_2$ and 1.6 g $Cu(acac)_2$, respectively. The unmodified (Ce/Zn) was designated as 0 %Cu(Ce/Zn). The incipient wet impregnation (IWI) strategy was developed here to precisely optimize the catalyst's structure and surface properties. IWI has been demonstrated to enhance catalytic activity and selectivity for propene during the CO_2-ODHP reaction [15].

2.3. Catalyst characterizations

High-angle annular dark-field transmission electron microscopy (HAADF-TEM) and elemental mapping by means of energy-dispersive X-ray spectroscopy (EDS) were conducted in a NIPPON Electronics 2100 microscope operated at 200.0 kV to analyze the morphological shapes and bulk elemental configurations of the as-prepared catalyst. Raman spectra of the catalysts were recorded with a HORIBA Model LabRAM HP evolution Raman spectrometer, covering the range of 200–1200 cm^{-1} using a 525.0 nm laser at room temperature. The specific surface area of each sample was determined by N_2 physisorption at 77.35 K conducted in an Autosorb iQ Canta apparatus (Quantachrome); the resulting adsorption-desorption isotherms (see Fig. S2 in the supplementary material (SM)) were evaluated employing the Brunauer-Emmett-Teller (BET) method. X-ray diffraction (XRD) patterns were obtained using a RIGAKU ULTIMA IV X-ray diffraction instrument with Cu Kα radiation, scanning from 5.0° to 90.0°. X-ray photoelectron spectroscopy (XPS) was employed to discover surface chemical compositions and ionic states on a Thermo Fly's NEXSA, utilizing a 1486.8 eV excitation voltage and a 15.0 kV assessment voltage. Temperature-programmed reduction with hydrogen (H_2-TPR) was performed using Micromeritics AutoChem II 2920 equipment to evaluate the reducibility characteristic of the samples. Finally, the optical properties were assessed at room temperature with a SHIMADZU UV-2600i visible-near-infrared spectrophotometer, spanning wavelengths from 200 to 800 nm. Thermogravimetric analysis (TGA) was carried out on a NETZSCH STA 409 C/CD instrument. After loading 25.0 mg sample, the temperature was increased to 600 °C with a ramp rate of 10 °C min^{-1} in N_2 flow (50 mL min^{-1}). All characterization analyses were conducted on the as-prepared catalysts, except for the TGA, which was performed on the spent catalyst.

2.4. Catalytic testing

Catalytic tests for CO_2-ODHP were conducted with a fixed-bed placed in a horizontal quartz glass tubular reactor, with an internal diameter of 0.8 cm and a length of 90.0 cm, heated by a furnace (1200 °C Single Temperature Zone Stainless Steel Vacuum Atmosphere Tubular Electric Furnace from Tianjin Zhonghuan Electric Furnace Co., Ltd., China) (see Fig. S1 in the SM). Each test involved placing 0.2 g of the as-prepared Cu (Ce/Zn) catalyst powder into the reactor tube, resulting in a catalyst bed height of ~3.0 mm. The as-prepared catalysts were initially pre-reduced using a mixture of H_2 and Ar at a flow rate of 40.0 mL min^{-1} for 1 h at 550 °C, then cooled to 250 °C, to eliminate any adsorbents on the surface of the catalyst before performing the catalytic test. Subsequently, a gas mixture consisting of 4.0 mL min^{-1} C_3H_8, 8.0 mL min^{-1} CO_2, and 28.0 mL min^{-1} Ar was introduced into a reactor, maintaining a total flow rate of 40.0 mL min^{-1} (Gas Hourly Space Velocity (GHSV) = 12,000 h^{-1}) while gradually increasing the temperature in increments of 50 °C, from 250 °C to 550 °C. The products were analyzed using an online gas chromatograph (GC7890B, Agilent Technologies) equipped with a flame ionization detector (FID, Porapak Q column) and a thermal conductivity detector (TCD, TDX-01). After each 50 °C temperature increment, the conversion of propane and CO_2, the selectivity for the products CH_4, C_2H_4, and C_3H_6, as well as the C_3H_6 yield, were assessed using Eqs. (1)–(4). The ratio for the consumption rate of CO_2 to that of C_3H_8 is given in Eq. (5). Blank tests were conducted under the same reaction conditions but in an empty reactor without a catalyst bed, and by means of these blank tests, gas phase reactions were found to be irrelevant. The mass and heat transfer diffusion limitation on the as-prepared catalysts has been assessed based on the Weisz-Prater and Mears criteria [16] presented in Section 2 in the SM.

$$C_3H_8\text{conversion}\ (\%) = \frac{F(C_3H_8)_{in} - F(C_3H_8)_{out}}{F(C_3H_8)_{in}} \times 100 \quad (1)$$

$$CO_2 \text{conversion}\ (\%) = \frac{F(CO_2)_{in} - F(CO_2)_{out}}{F(CO_2)_{in}} \times 100 \quad (2)$$

Selectivity of product S_i (%) was calculated as follows:

$$S_i(\%) = \left(\frac{n_i\ (F_i)_{out}}{F(C_3H_8)_{in} - F(C_3H_8)_{out}} \right) \times 100 \quad (3)$$

$$C_3H_6\ \text{yield}\ (\%) = \frac{F(C_3H_6)_{out}}{F(C_3H_8)_{in}} \times 100 \quad (4)$$

$$r(CO_2)/r(C_3H_8) = \left(\frac{F(CO_2)_{in} - F(CO_2)_{out}}{F(C_3H_8)_{in} - F(C_3H_8)_{out}} \right) \quad (5)$$

The propane reaction rate by mass and the turnover frequency (TOF) were determined as follows in Eqs. (6) & (7), respectively:

$$\text{Reaction rate}\ \left(\text{mol}\ g_{cat}^{-1} s^{-1}\right) = \frac{X(C_3H_8) \times 60 \times F(C_3H_8)_{in}}{22.4 \times m_{cat}} \quad (6)$$

$$\text{TOF}\ \left(s^{-1}\right) = \frac{F(C_3H_8)_{in} \times X(C_3H_8) \times M_{Cu}}{60 \times 22.4 \times m_{cat} \times C(Cu_{active})} \quad (7)$$

The stability of the catalyst was quantified using the relative deactivation rate, defined as follows in Eq. (8):

$$\textit{Relative deactiation rate}\ (\%) = \frac{Y_{20} - Y_{360}}{Y_{20}} \times 100 \quad (8)$$

The carbon balance for each catalyst at 550 °C was evaluated using Eq. (9):

$$(\%) = \frac{\left[F_{CH_4}\right]_{out} + 2\times\left[F_{C_2H_4}\right]_{out} + 2\times\left[F_{C_2H_6}\right]_{out} + 3\times\left[F_{C_3H_6}\right]_{out} + 3\times\left[F_{C_3H_8}\right]_{out} + \left[F_{CO}\right]_{out} + \left[F_{CO_2}\right]_{out}}{3\times\left[F_{C_3H_8}\right]_{in} + \left[F_{CO_2}\right]_{in}} \times 100 \quad (9)$$

The XPS species ratios were calculated following Eqs. (10)–(12):

$$Ce^{3+}/Ce^{4+} = \frac{\textit{Relative percentage area of}\ Ce^{3+}}{\textit{Relative percentage area of}\ Ce^{4+}} \quad (10)$$

$$Cu^{2+}/Cu^{+} = \frac{\textit{Relative percentage area of}\ Cu^{2+}}{\textit{Relative percentage area of}\ Cu^{+}} \quad (11)$$

$$O_{Lat}/O_{Ads} = \frac{\textit{Relative percentage of}\ O_{Lat}}{\textit{Relative percentage of}\ O_{Ads}\ \left(CO_3^{2-} + OH^-\right)} \quad (12)$$

Herein, $F(C_3H_8)$ and $F(CO_2)$ represents the volumetric flow rates (mL min^{-1}) of C_3H_8 and CO_2, respectively, which are regulated and measured by using a mass flow controller; the indices "in" and "out" correspond to the inlet and oulet values, respectively. To facilitate the measurement of outlet flow rates for different species, 4.0 vol.% Ar was co-fed with the reactants as an internal standard. The flow rate and carbon number of product i, which includes CH_4, C_2H_6, C_2H_4, and C_3H_6, are denoted as F_i and n_i, respectively. The consumption rates for CO_2 and C_3H_8 are indicated by $r(CO_2)$ and $r(C_3H_8)$, respectively. The conversion of C_3H_8 is represented by $X(C_3H_8)$, while m_{cat} denotes the weight of the catalyst. The content of active copper atoms on the catalyst is denoted by $C(Cu_{active})$, and M(Cu) represents the molar mass of a copper atom. Y_{20} and Y_{360} indicate the yield of C_3H_6 at time on stream (TOS) of 20 and 360 min, respectively.

2.5. Computational details

Density functional theory (DFT) calculations were carried out to evaluate the CO_2 adsorption structures and energies over the CeO_2/CuO/ZnO surface model. First, a Periodic CeO_2 (111) surface model was established, onto which a CuO-ZnO cluster was placed. The DMol^3 package facilitated the calculation process [17]. The generalized gradient approximation (GGA), along with the Perdew–Burke–Ernzerhof (PBE) approach, was employed to characterize the correlation and exchange potential [18]. The inner core electrons were evaluated using the DFT Semi-core Pseudopotential approach, and the Double Numerical plus Polarization (DNP) basis set was selected for the calculations. To improve convergence, a smearing value of 0.05 eV was applied. CeO_2 has a space group number of Fm-3m (225) with a fluorite structure. A 4 × 4 × 4 k-point mesh was employed for the optimization of the crystal geometry. The perfected CeO_2 crystal was used, and the optimized lattice constant was a = b = c = 5.4892 Å, and angles $\alpha = \beta = \gamma = 90^\circ$ A CeO_2 (111) surface slab was cleaved from the optimized CeO_2 (111) surface slab with a 2 × 2 surface supercell. A 15 Å vacuum layer is placed above the surface plane to avoid interference from imaging surface planes. For the surface slab calculations, the k-point uses a 4 × 4 × 1 Monkhorst-Pack k-point grid.

The interplay between the CO_2 adsorbate and the catalyst's surface is characterized by the adsorption energy (E_{ad}). This energy is evaluated via the following Eq. (13):

$$E_{ad} = E_{sys} - E_{ads} - E_{sur} \quad (13)$$

Herein, E_{sys} represents the system's energy after adsorption, E_{ads} denotes the energy of the adsorbate prior to adsorption, and E_{sur} indicates the energy of the surface adsorption.

3. Results

3.1. Crystallite structure & textural properties

The phases of the catalysts were analyzed by using XRD to comprehend the nature of their crystalline growth and clarify their structures. Fig. 1a presents the XRD peaks recorded for the as-prepared catalysts. The XRD patterns reveal sharp and narrow peaks, demonstrating the existence of crystalline structures in all four catalysts. The copper-free catalyst designated as 0 %Cu(Ce/Zn) is associated with a combination of hexagonal zinc oxide (ZnO, JCPDS No 01-075-0576), cubic cerium zinc (CeZn, JCPDS No 03-065-1805), and the cubic cerium oxide (CeO_2, JCPDS No 01-089-8436). The three other catalysts, which contain copper and are labelled as 1 %Cu(Ce/Zn), 2 %Cu(Ce/Zn) and 3 %Cu(Ce/Zn), correspond to a mixture of monoclinic copper oxide (CuO, JCPDS No 01-080-1917), rhombohedral copper zinc (CuZn, JCPDS No 00-026-0571), orthorhombic cerium copper (CeCu, JCPDS No 00-025-1138), hexagonal zinc oxide (ZnO, JCPDS No 01-075-0576), cubic cerium zinc (CeZn, JCPDS No 03-065-1805), and cubic cerium oxide (CeO_2, JCPDS No 01-089-8436).

Using the intense reflexes and applying Debye-Scherrer's equations (Eqs. (14) & (15)) as shown in Table S1 (see SM), the crystallite sizes (D) were evaluated to be 15.2, 16.2, 19.4, and 21.1 nm (±0.3 nm), while the micro-strain (ε) values were determined to be 0.15, 0.13, 0.11 and 0.10 % (± 0.03 %) for the samples of 3 %Cu(Ce/Zn), 2 %Cu(Ce/Zn), 1 %Cu(Ce/Zn), and 0 %Cu(Ce/Zn), respectively.

$$D = 0.9\ \lambda/\beta\ \cos\theta, \quad (14)$$

$$\varepsilon = \beta/2\cot\theta, \quad (15)$$

where β is the diffraction widening at half-height for Bragg's angle θ, and λ denotes the wavelength of the X-ray radiation.

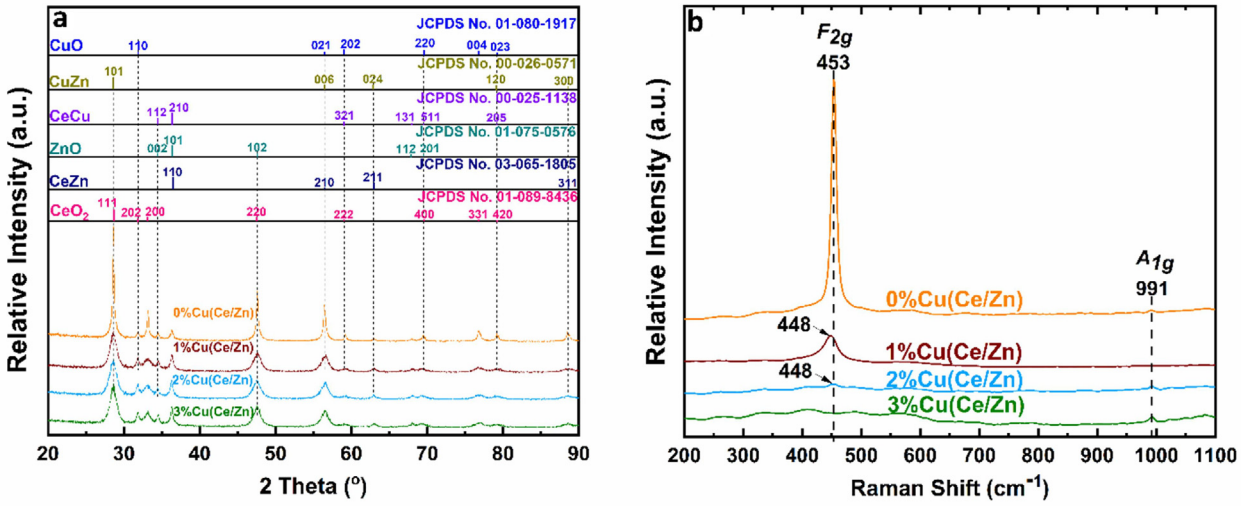

Fig. 1. XRD patterns (a) and Raman spectra (b) of the as-prepared catalysts.

The crystallite size of the samples decreases as the Cu loading within the (Ce/Zn) structure increases. This reduction in crystallite size could be attributed to the reconfiguration of ions in the crystalline matrix of the (CeZn). Shannon et al. [19] found that the ionic radius (r_{ionic}) and crystal radius ($r_{crystal}$) of Cu^{2+} (0.57 Å and 0.71 Å, respectively) are smaller than those of Ce^{3+} (Ir: 1.14 Å, Cr: 1.28 Å) and Zn^{2+} (Ir: 0.60 Å, Cr: 0.74 Å), respectively. Consequently, the crystallite sizes of 1 %Cu(Ce/Zn), 2 %Cu(Ce/Zn), and 3 %Cu(Ce/Zn) are smaller than that of 0 %Cu(Ce/Zn), with 3 %Cu(Ce/Zn) exhibiting the smallest crystallite size. These characterization data are relevant to the present study, because the crystallite size substantially affects the catalytic activity according to previous research [20,21], and thus, the smaller crystallite size observed in this work for Cu-containing samples may govern propane conversion in CO_2-ODHP.

Fig. 1b depicts the Raman spectra of the as-prepared catalysts, obtained using a 525 nm laser at room temperature. Two prominent peaks are observed at ~453 cm^{-1} and ~991 cm^{-1}. The peak at ~453 cm^{-1} relates to the triply degenerate F_{2g} mode of CeO_2. Upon copper-incorporation into (Ce/Zn) lattice, this peak exhibits a decrease in intensity and a notable blue shift from 453 to 448 cm^{-1}, which can be attributed to changes in lattice arrangement: the intermediary doping of CuO into the (Ce/Zn) network leads to the formation of oxygen vacancies (O_v) [22], resulting in lattice growth and mode softening. As uncovered by XRD analyses, each vacancy is formed by the substitution of two Ce^{3+} ions (ionic radius 1.14 Å) for two Ce^{4+} ions (0.97 Å). [23]. The second band at ~991 cm^{-1} (A_{1g}) is associated with oxygen vacancies and is particularly pronounced in the spectrum of the 3 %Cu(Ce/Zn) sample. This peak originates from a D-lattice defect triggered by an oxygen vacancy [24]. Complementary XPS analyses indicate that Cu doping promotes a conversion from Ce^{4+} to Ce^{3+}, leading to an increased number of O_v [25]. The Raman shift alteration between the D-peak (900 cm^{-1}) and the F_{2g} peak (453 cm^{-1}) is approximately 447 cm^{-1}, suggesting that the oxygen vacancies in the Cu(Ce/Zn) catalysts are produced by intrinsic defects $Ce^{4+} \rightarrow Ce^{3+}$ [26]. From the perspective of the catalysis, it is crucial to investigate the presence of oxygen vacancies (O_v), as their formation is linked to the presence of Ce^{3+} [27]. The literature presents two mechanistic scenarios [27]. In the first scenario, when the lattice oxygen leaves its original position, two electrons from the vacant site localize on two Ce^{4+} ions, reducing them to form Ce^{3+}–O_v–Ce^{3+} pairs [28]. In the second scenario, one electron from the lattice oxygen localizes on a Ce^{4+}, resulting in Ce^{4+}–O_v–Ce^{3+} species. In this case, the other electron is trapped in a position adjacent to the vacancy, leading to the generation of an F^+ center [28].

Table 1
Specific surface area of the as-prepared samples.

Catalysts	Surface area (m^2 g^{-1})	Pore volume (cm^3 g^{-1})	Pore size (nm)
0 %Cu (CeZn)	9.6	0.02	3.812
1 %Cu (CeZn)	16.9	0.03	3.819
2 %Cu (CeZn)	18.5	0.04	3.821
3 %Cu (CeZn)	19.6	0.05	3.831

The N_2-physisorption results obtained according to the BET method are shown in Table 1 and reveal the specific surface area (SSA) of the samples: 9.6, 16.9, 18.5, and 19.6 ± 0.2 m^2 g^{-1} for 0 %Cu(Ce/Zn), 1 %Cu(Ce/Zn), 2 %Cu(Ce/Zn), and 3 %Cu(Ce/Zn), respectively. The corresponding pore volumes are 0.02, 0.03, 0.04, and 0.05 ± 0.005 cm^3 g^{-1}, respectively. The N_2 adsorption-desorption isotherms and the pore size distribution for the as-prepared catalysts are depicted in Fig. S2 (see SM). The data indicate that increasing the Cu content improved both the SSA and pore volume of the nanopowder catalysts. These findings align with the crystallite size trends identified in the XRD data. As mentioned above, a smaller crystallite size, along with a larger SSA and pore volume, benefits the mobility of oxygen and active sites, and can promote the catalytic performance [29]. Consequently, doping (Ce/Zn) with Cu is expected to be advantageous for CO_2-ODHP, and 3 %Cu(Ce/Zn) is anticipated to exhibit the highest activity.

3.2. Morphology and bulk chemical composition

Fig. 2 displays the TEM and HRTEM microscopy images of the Cu(CeZn) samples. The catalysts disclose hexagonal-like morphologies with spherical shapes akin to those of the Cu/Zn-O_v-Ce synthesized by Ye et al. [23]. Color mapping images based on EDS analysis indicate a high dispersion of nanoparticles for high Cu loading and reveal that the Cu(Ce/Zn) sample displays a homogeneous distribution of Cu, Zn, and Ce metals, as illustrated in Figs. S3 and S4 (see SI). Table S2 (see SM) provides the relative composition of Cu(CeZn) ternary oxides as determined by EDS and XPS. These findings align with the XRD and BET results, which show a decrease in crystallite grain size alongside an increase in specific surface area and pore volume with higher Cu concentrations in the catalyst structure. Literature suggests that the aggregation of tiny particles enhances large pore volumes and facilitates abundant oxygen movement, which is essential for propane oxidation [30]. Hence, a catalyst with a higher Cu proportion is expected to show improved catalytic performance.

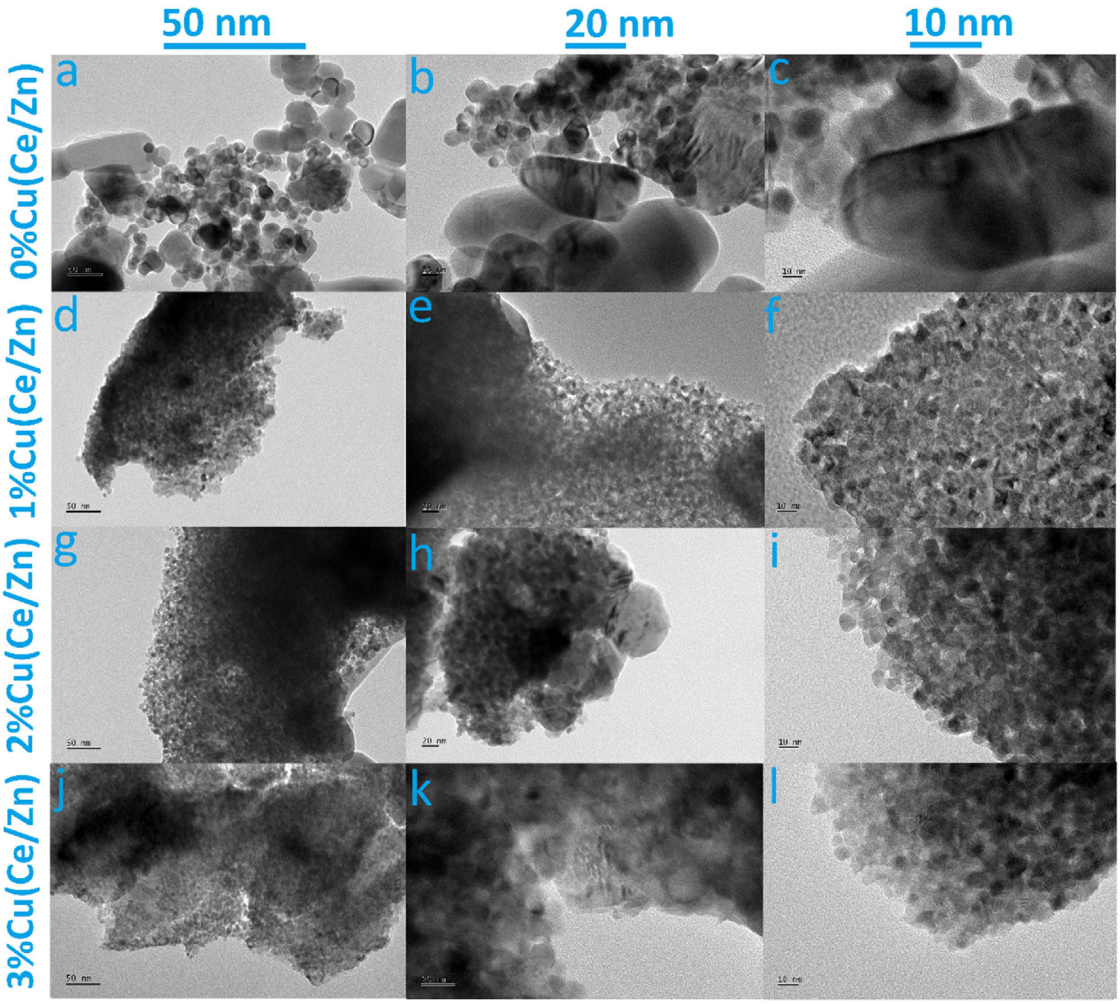

Fig. 2. TEM (50 nm), and HRTEM (20 nm and10 nm) of CeZn catalysts samples with various Cu loading. 0 %Cu(Ce/Zn) (a, b, c), 1 %Cu(Ce/Zn) (d, e, f), 2 %Cu(Ce/Zn) (g, h, i), and 3 %Cu(Ce/Zn) (j, k, l).

3.3. Elemental composition and oxidation state analysis

The XPS analysis was conducted to investigate the chemical constituents and ionic state of the catalyst surface. Fig. 3a–d elucidate the XPS spectra of the Ce 3*d* regions in the as-prepared catalysts. The deconvolution of the Ce 3*d* spectra reveals two spin-orbitals, $3d_{5/2}$ and $3d_{3/2}$, which are further split into six distinct peaks. The peaks at 883.45–883.98 eV and 900.27–900.89 eV (±0.2 eV) correspond to the trivalent cerium ion (Ce^{3+}), while those at 882.08–882.19 eV and 898.02–898.24 eV (±0.2 eV) are associated with the tetravalent cerium ion (Ce^{4+}). The asymmetric nature of the Ce 3*d* spectra indicates the coexistence of Ce^{3+} and Ce^{4+} species, in agreement with previous work [31]. The Ce species are primarily identified as CeO_2 and Ce_2O_3, with CeO_2 being the most prominent, as indicated by the XRD peaks. The proportional rates of Ce^{4+} and Ce^{3+}, detailed in Table S3 (see SM), were evaluated based on the XPS peak areas. The Ce^{3+}/Ce^{4+} ratio increases significantly if copper is added to the (Ce/Zn) lattice, with the 3 %Cu(Ce/Zn) sample having the highest Ce^{3+}/Ce^{4+} ratios of 2.3 and 2.5 for Ce $3d_{5/2}$ and Ce $3d_{3/2}$, respectively. This trend suggests a higher presence of Ce^{3+} and an increased quantity of oxygen vacancies, which play a crucial function in the oxidation reaction, as previously stated [12].

Fig. 3e–h depict the XPS spectra of Zn 2*p*. The Zn 2*p* core level spectrum reveals a doublet range from 1017 to 1025 eV (±0.3 eV) for Zn $2p_{3/2}$ and from 1042 to 1047 eV (±0.3 eV) for Zn $2p_{1/2}$ [32]. The deconvolution of the Zn $2p_{3/2}$ spin orbitals generates three characteristic peaks, corresponding to three species, namely Zn^0, ZnO, and $Zn(OH)_2$ [9]. The proportional ratios of these species are summarized in Table S4 (see SI). As shown in Table S4 (see SM), incorporating Cu into Ce/Zn increases the quantity of ZnO (from 78.7 % to 96.1 %), which is in line with the findings from XRD investigations. Notably, the second significant peak, Zn $2p_{1/2}$, indicates that the 3 %Cu(Ce/Zn) catalyst contains the highest concentration of Zn^{2+}. Previous studies emphasized that Zn^{2+} plays a crucial role in CO_2-ODHP [9].

Fig. 3i–l present the O 1*s* binding energy (BE) regions for all samples. The O 1*s* core-shell spectrum displays a prominent peak in the BE range of 528–532 eV (±0.1 eV). After deconvoluting this main peak, several features emerge, indicating the presence of various oxygenated species related to adsorbed oxygen (O_{Ads}) and lattice oxygen (O_{Lat}) on different catalyst surfaces. Irrespective of the catalyst composition, the peaks at 529.13, 529.19, 529.24, and 529.36 eV (±0.1 eV) are attributed to O_{Lat} (O^{2-}). However, the introduction of Cu into (Ce/Zn) increases the amount of lattice oxygen (O^{2-}) from 24.08 % for 0 %Cu(Ce/Zn) to 32.74 % for 3 %Cu(Ce/Zn), confirming that the latter catalyst contains the highest amount of O_{Lat}. Additionally, literature suggests that the peaks in the range of 530 to 536 eV (±0.1 eV) can be assigned to oxygen-containing species adsorbed on the catalyst surface, such as OH^- and CO_3^{2-} [2]. The highest O_{Lat}/O_{Ads} ratio of 0.49 is observed in the 3 %Cu(Ce/Zn) sample, whereas this ratio is lower for the other samples: 0.43 for 2 %Cu(Ce/Zn), 0.39 for 1 %Cu(Ce/Zn), and 0.32 for 0 %Cu(Ce/Zn) (see Table S5 in SM). The increase in O_{Lat} on the catalysts'

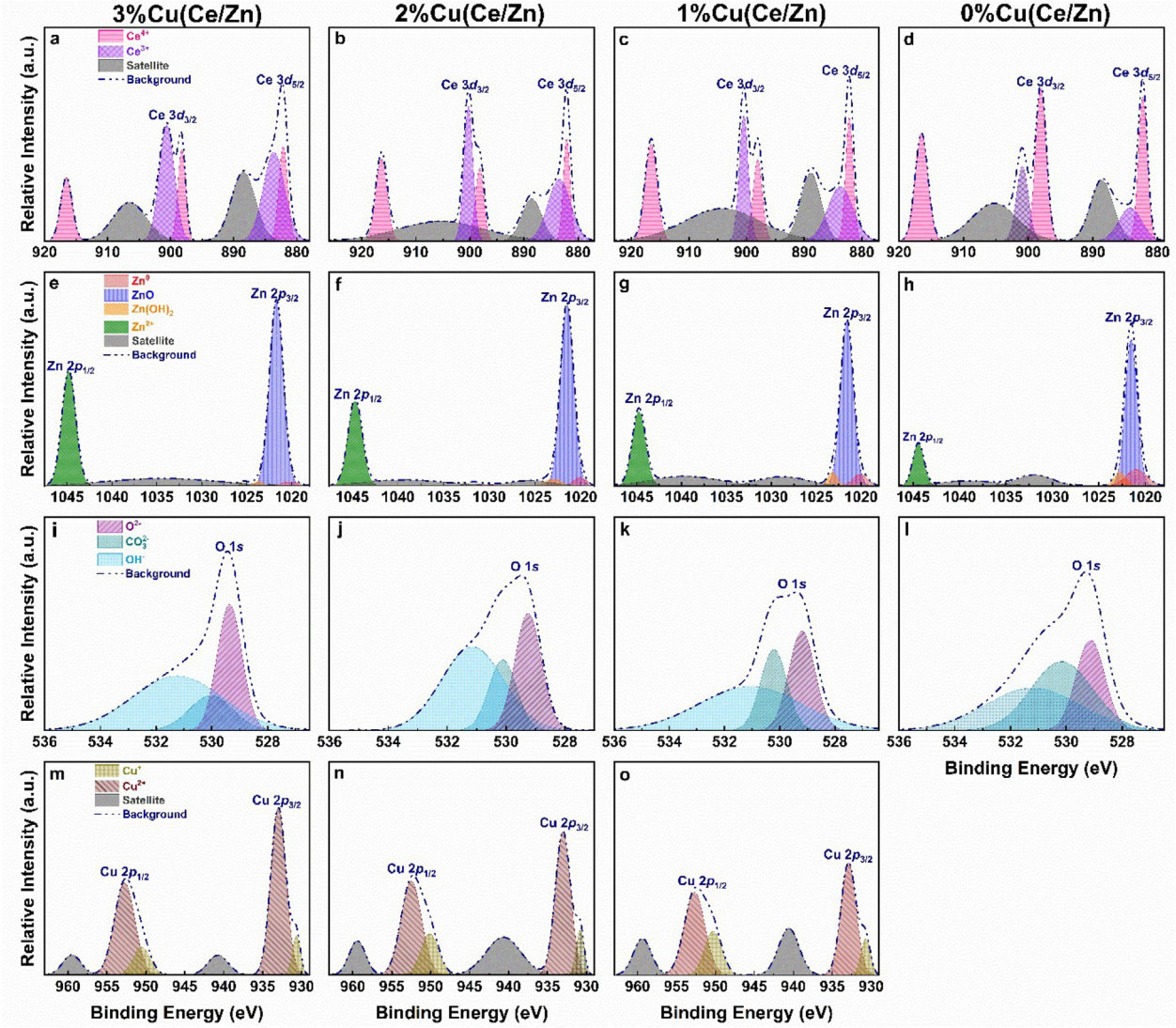

Fig. 3. Deconvoluted XPS spectra of the as-prepared catalysts. Ce 3*d* (a–d), Zn 2*p* (e–h), O 1*s* (i–l), and Cu 2*p* (m–o).

surfaces with increasing Cu loading into the (Ce/Zn) lattice could be attributed to the small crystallite size and large pore volume observed via XRD and BET analyses, respectively. According to Ansari et al. [33] and Samuel et al. [21], O_{Lat} (O^{2-}) plays a crucial role in CO_2-ODHP as it facilitates hydrogen abstraction from C–H bonds to form H_2O and reduces the higher valence states of metal oxides to lower valence oxides.

Fig. 3m–o display the XPS spectra of Cu 2*p*, revealing that the Cu 2*p* core-shell features two prominent peaks in the binding energy (BE) ranges of 928–937 eV (±0.1 eV) and 947–957 eV (±0.1 eV), conforming to Cu $2p_{3/2}$ and Cu $2p_{1/2}$, respectively. Each intense peak comprises two bands that can be attributed to the bivalent copper ion (Cu^{2+}) and the monovalent copper ion (Cu^{+}). The lower peaks of Cu $2p_{3/2}$, located at 932.91–933.01 eV (±0.1 eV), are associated with Cu^{2+} in octahedral sites [32]. The fitted XPS data for Cu 2*p* obtained through peak deconvolution are summarized in Table S6 (see SI). The highest ratios of Cu^{2+}/Cu^{+} of 8.2 and 3.9 for Cu $2p_{3/2}$ and Cu $2p_{1/2}$, respectively, are observed in the 3 %Cu(Ce/Zn) sample, implying a greater presence of more Cu^{2+} species at the surface; presumably, the majority of these surface Cu^{2+} species can get reduced to Cu^{+} species during the propane reaction. The presence of Cu^{2+} on the catalyst surface could significantly influence the propane catalytic reaction, which is in line with the literature [14]. The 3 %Cu(Ce/Zn) catalyst with more Cu^{2+} at the surface is expected to demonstrate enhanced catalytic oxidation.

Table 2
H_2-TPR reduction temperature data of the as-prepared samples.

Catalysts	Temperature (°C)	
	α	*β*
0 %Cu(Ce/Zn)	309	382
1 %Cu(Ce/Zn)	156	188
2 %Cu(Ce/Zn)	151	174
3 %Cu(Ce/Zn)	132	157

3.4. Redox properties

The redox properties of the samples were analyzed by means of H_2-TPR experiments over a temperature range of 50–800 °C. The H_2-TPR data are depicted in Fig. 4a. All samples exhibit two distinct groups of reduction peaks, occurring in the temperature ranges of 132–309 °C and 157–382 °C, corresponding to the *α*-type and *β*-type hydrogen reductions, respectively (see Tables 2 and S7 in the SM). Notably, the hydrogen consumption patterns for all four catalysts exhibit a similar shape, with significant reduction peaks within the 157–382 °C range (*β*-type). The 0 %Cu(Ce/Zn) sample showed two distinct peaks of differing intensities at 309 °C and 382 °C. With the introduction of 1 wt.% of

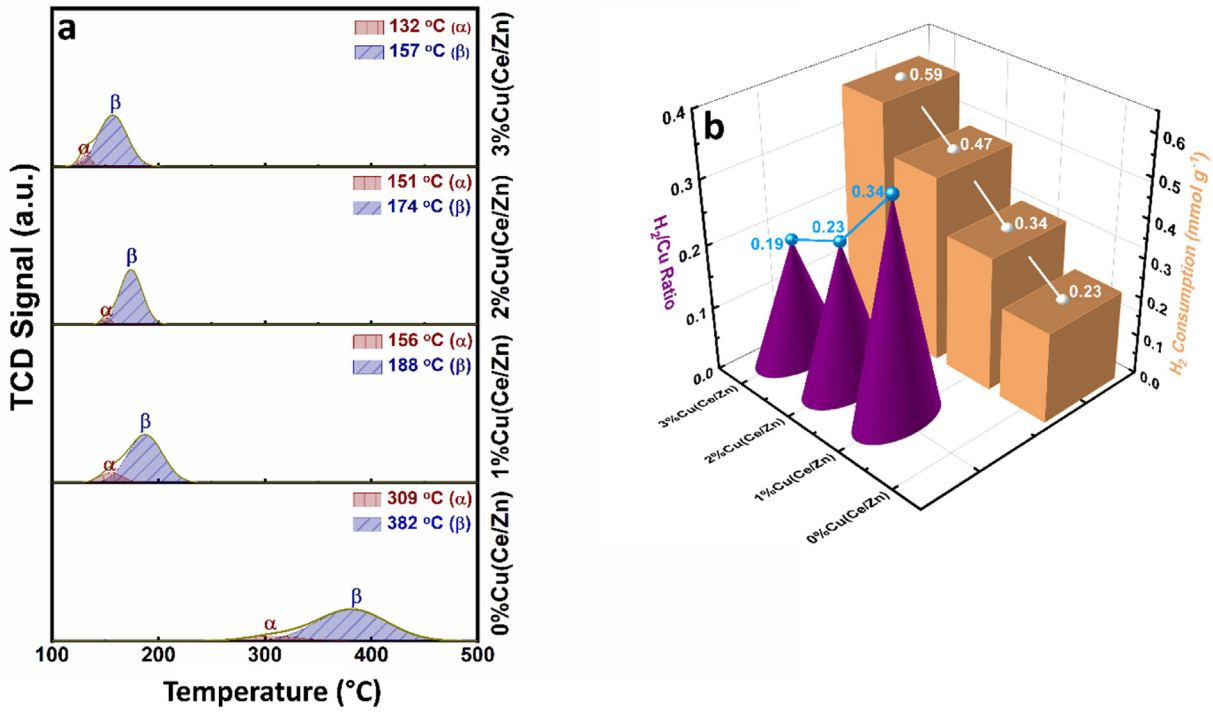

Fig. 4. H_2-TPR profiles of the as-prepared catalysts.

copper, a notable decrease was observed, with the α-type peak shifting from 309 °C to 156 °C and the β-type peak shifting from 382 °C to 188 °C. Furthermore, as the Cu loading increases from 2 % to 3 %, the high-temperature adsorption peaks are shifted to lower temperatures, with the α-type, and β-type ranges ranging from 309 °C to 132 °C and from 382 °C to 157 °C, respectively, because of the enhanced dispersion of Cu within the (Ce/Zn) lattice. Previous reports have indicated that the temperature programmed reduction (TPR) peaks in the 300–400 °C range are associated with the steady reduction of surface Ce^{4+} to Ce^{3+} [34], whereas those in the 130–200 °C range correspond to the reduction of Cu^{2+} to Cu^{+} [35]. The 3 %Cu(Ce/Zn) catalyst was reduced at a lower temperature than the other three catalysts, suggesting it possesses the highest intrinsic reducibility.

To assess the number of Cu^{2+} oxides over the Cu(Ce/Zn) catalysts, the quantity of consumed H_2 and its ratio to Cu were evaluated through the integration of the TCD signal obtained during the H_2-TPR experiments; the results are summarized in Fig. 4b. The quantity of consumed H_2 increases nearly linearly from 0.23 to 0.59 (±0.03) mmol g^{-1} as the Cu loading rises from 0 wt.% to 3 wt.% over (Ce/Zn). In terms of the H_2/Cu molar ratio, it decreases continuously from 0.34 to 0.19 (±0.03) with the increment in Cu loading over (Ce/Zn) from 0 wt.% to 3 wt.%, which corresponds to the observed pattern of consumed H_2. Therefore, the reductive characteristics of Cu^{2+} oxides on Cu(Ce/Zn) catalysts are highly influenced by Cu loading, indicating that the structure and composition of CuO_x oxides on Cu(Ce/Zn) vary with different Cu loadings.

3.5. Optical properties

The adsorption spectra of the catalysts and Tauc's plot, which display an approximate bandgap energy (E_g), were analyzed, and the findings are presented in Fig. 5. Fig. 5a illustrates a decrease in adsorption as the wavelength expands into the visible area. All the as-prepared samples exhibit a prominent peak at ~279 nm. For the 0 %Cu(Ce/Zn) sample, this peak is attributed to the O → Ce^{3+} charge transfer [36]. In contrast, for the other three catalysts containing copper, this peak results from an overlap of the O → Ce^{3+} charge transfer and the charge transfer band from the 2*p* levels of O^{2-} to the 3*d* orbitals of Cu^{2+} [25]. Additionally, all four catalysts display a significant band at ~360 nm, which is due to the charge transfer from O^{2-} (2*p*) to Zn^{2+} (3*d*), which points to the existence of bulk ZnO [37]. For 1 %Cu(Ce/Zn), 2 %Cu(Ce/Zn), and 3 %Cu(Ce/Zn) catalysts, a third peak is observed at ~692 nm, corresponding to the d–d transitions of Cu^{2+} [25]. The optical E_g derived from the adsorption spectra was calculated using Tauc's equation (Eq. (16)), which relates the incident photon energy ($h\nu$) to the adsorption coefficient (α):

$$\alpha h\nu = A\left(h\nu - E_g\right)^n, \tag{16}$$

where A is a constant representing the refractive index, and n is a constant that describes the nature of the transition (in this study, $n = 2$, as the samples exhibited a direct bandgap).

The corresponding Tauc plot of $(\alpha h\nu)^2$ for the different catalysts is shown in Fig. 5b. The E_g for each sample was determined from the intersection of the direct line with the photon energy $h\nu$ axis. The E_g values were evaluated to be 1.71, 1.85, 2.01, and 2.73 ± 0.05 eV for the 3 %Cu(Ce/Zn), 2 %Cu(Ce/Zn), 1 %Cu(Ce/Zn), and 0 %Cu(Ce/Zn) samples, respectively. The 3 %Cu(Ce/Zn) sample has the smallest E_g, which corresponds to a high quantity of O_{Lat} and thus supports the data from XPS analysis. Lower E_g correlates with increased mobility of O_{Lat}, enhancing the catalytic performance during propane oxidation [3].

3.6. Catalytic performance

The results of the CO_2-ODHP reactions using Cu(Ce/Zn) catalysts are depicted in Fig. 6. The initial conversion of both C_3H_8 (Fig. 6a) and CO_2 (Fig. 6b) correlates with the Cu-loading: while at a time on stream (TOS) of 20 min the Cu-free sample exhibits the lowest C_3H_8 and CO_2 conversion of 38.8 % and 6.0 %, respectively, the 3 %Cu(Ce/Zn) catalyst performs best and converts 46.9 % C_3H_8 and 8.4 % CO_2. In contrast, 0 %Cu(Ce/Zn) has the highest initial C_3H_6 selectivity of 57.0 %, whereas the Cu-containing samples exhibit slightly lower selectivities ranging from 54.9 % to 57.3 % for 1 %Cu(Ce/Zn) and 3 %Cu(Ce/Zn), respectively (Fig. 6c). Consequently, the initial C_3H_6 yields follow the order of 0 %Cu(Ce/Zn) < 1 %Cu(Ce/Zn) < 2 %Cu(Ce/Zn) < 3 %Cu(Ce/Zn) (Fig. 6d); a maximum C_3H_6 yield of 25.2 % is achieved over 3 %Cu(Ce/Zn).

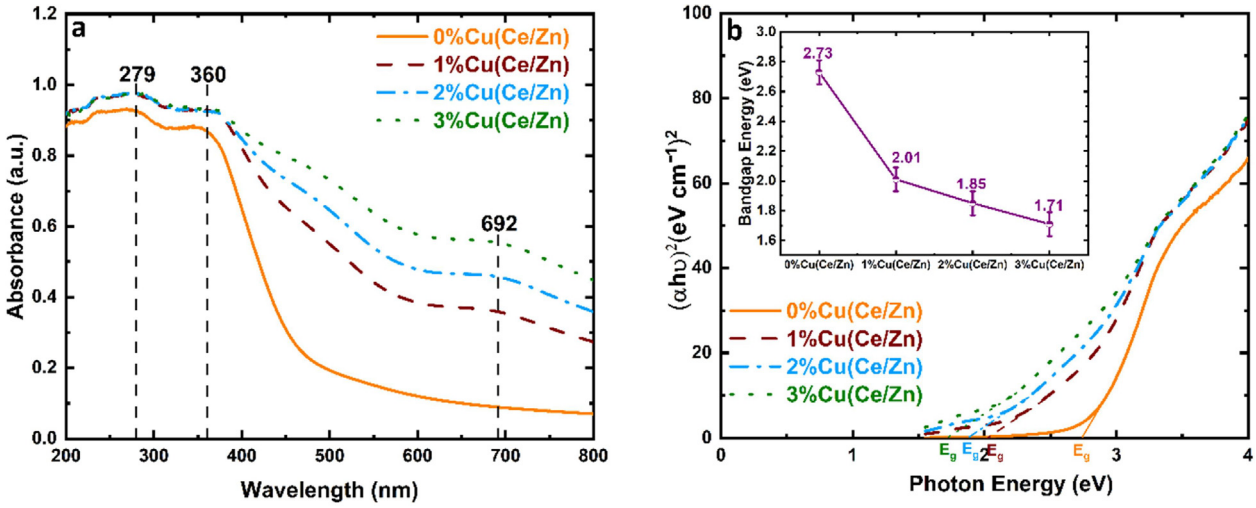

Fig. 5. UV-vis absorption spectra (a), $(\alpha h\nu)^2$ versus $h\nu$, and bandgap energies of the catalysts (b).

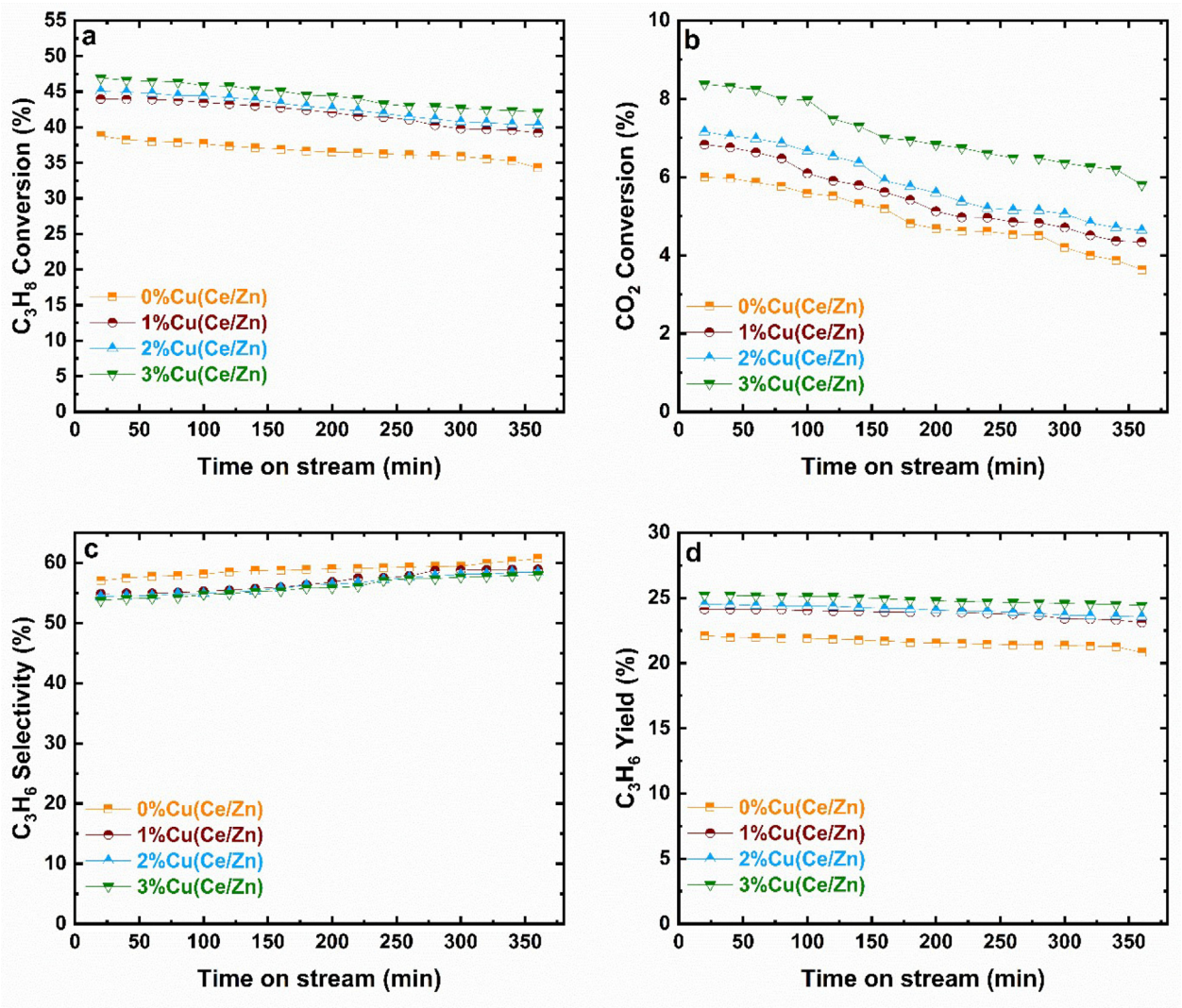

Fig. 6. The time-on-stream conversions of C_3H_8 (a) and CO_2 (b), the C_3H_6 selectivity (c), and the C_3H_6 yield (d) for CO_2-ODPH catalyzed by Cu(Ce/Zn). GHSV = 12,000 h^{-1}, and gas composition: 4 % C_3H_8, 8 % CO_2, diluted in Ar. T = 550 °C.

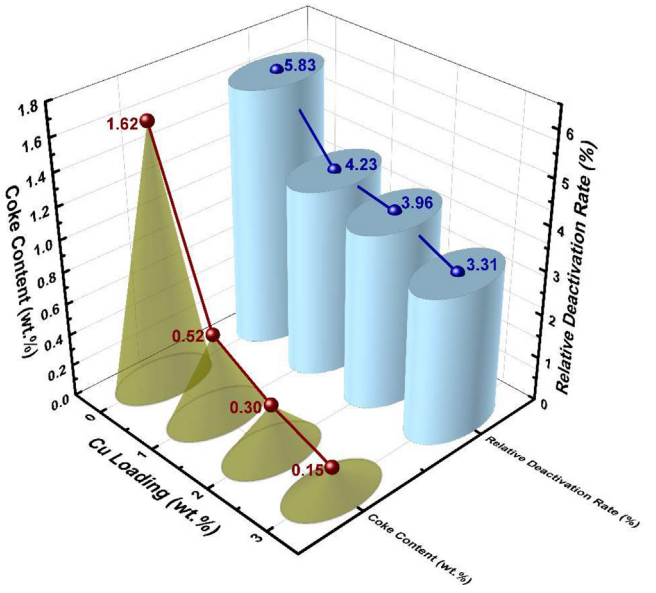

Fig. 7. The relative deactivation rate and the coke content as a function of the Cu loading over Cu(Ce/Zn) catalysts.

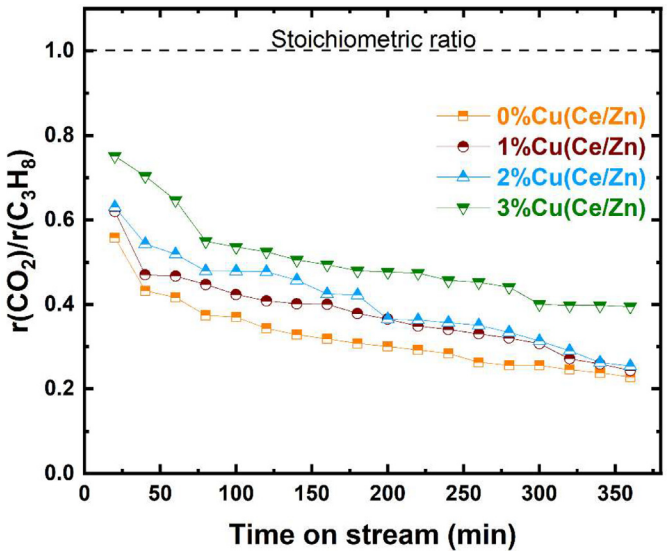

Fig. 8. The ratio for the consumption rate of CO_2 to that of C_3H_8 over Cu(Ce/Zn) catalysts as a function of time-on-stream.

The TOS results reveal that the performance of all catalysts declines over time, notably at similar rates. Using C_3H_8 conversion as an index, catalyst deactivation primarily takes place during the initial stages of the reaction, approximately within the first hour of TOS. While the TOS trends for CO_2 conversion closely resemble those for C_3H_8 conversion, a more significant dependence on the catalyst is evident. Notably, the CO_2 conversion decreases more rapidly with the increment in TOS for Cu(Ce/Zn) with a Cu loading of 1–3 wt.% compared to the Cu-free catalyst. In contrast, C_3H_6 selectivity gradually increases with longer TOS, irrespective of the catalyst formulations. To quantitatively assess the stability of the catalysts in CO_2-ODHP, the relative deactivation rate was calculated. This is defined as the variance between the initial (TOS = 20 min) and final (TOS = 360 min) C_3H_6 yields, divided by the initial yield. The findings are presented in Fig. 7. Consistent with a simple visual evaluation of the data depicted in Fig. 6, all catalysts demonstrate comparatively stable activity, with the highest and lowest relative deactivation rates being < 6 % for 0 %Cu(Ce/Zn) and 4 % for 3 %Cu(Ce/Zn), respectively. Therefore, the stability for CO_2-ODHP decreases in the following order: 0 %Cu(Ce/Zn) < 1 %Cu(Ce/Zn) < 2 %Cu(Ce/Zn) < 3 %Cu(Ce/Zn).

As depicted in Fig. 6c, the selectivity for C_3H_6 across all catalysts ranges from 53% to 60 %. Additionally, Fig. S5 (see SM) indicates that the carbon balance for all experiments is maintained within 96 ± 2 %. To identify the primary side reactions, the TOS selectivity of the detected gaseous by-products was evaluated, with results presented in Fig. S6 (see SM). Regardless of the Cu loading, CH_4, C_2H_6, and C_2H_4 consistently emerge as the main by-products across all the samples subject to this study. Furthermore, the TOS trends for the selectivity of CH_4 and C_2H_4 exhibit an inverse relationship compared to those for C_3H_6 and C_2H_6, aligning well with the carbon balance pattern displayed in Fig. S5 (see SM). Notably, the selectivity for C_2H_6 is higher than that for CH_4 and C_2H_4. It is important to mention that selectivities for C_2H_6 and CH_4 are significantly higher over the 3 %Cu(Ce/Zn) catalyst, whereas the 0 %Cu(Ce/Zn) catalyst shows the higher selectivity for C_2H_4. Considering the reaction temperature of 550 °C and a comparatively high GHSV of 12,000 h^{-1}, the cracking or hydrocracking of C_2H_6 and C_2H_4 to produce CH_4 could be deemed negligible. Hence, alongside the C_3H_6 selectivity results (Fig. 6c), the production of by-products over Cu(Ce/Zn) is primarily attributed to the cracking or hydrocracking of C_3H_8 and C_3H_6. Additionally, the slight difference in TOS selectivity among C_2H_6, C_2H_4, and CH_4 could be practically clarified by the effects of coke formation, resulting from the polymerization and cracking of adsorbed ethylene and propene on the catalyst surface. Consequently, product selectivity is influenced by the specific arrangement of the Cu(Ce/Zn) catalysts (Figs. 6c and S6), which will be further discussed along with the coking findings in a later section.

Given the simple redox behavior of CuO_x at high temperatures, it is widely proven that CO_2-ODHP over-supported CuO_x catalysts adhere to the Mars-van Krevelen redox pathway [14]. In this mechanism, the activated propane atoms extract active oxygen from CuO_x, in which Cu has a higher oxidation number, producing propene and water. Concurrently, CuO_x, in a reduced form in which Cu has a lower oxidation state, is re-oxidized by activated CO_2 atoms, completing the redox cycle of CuO_x while forming CO molecules. If the Mars-van Krevelen redox mechanism is assumed to be the only relevant process taking place during CO_2-ODHP, the stoichiometric reaction $C_3H_8 + CO_2 \leftrightarrow C_3H_6 + CO + H_2O$ would happen, resulting in a consumption rate ratio of CO_2 to C_3H_8 ($r(CO_2)/r(C_3H_8)$) of 1.0. Therefore, the proportion of $r(CO_2)/r(C_3H_8)$ over the different Cu(Ce/Zn) catalysts was evaluated as a function of time; the proportion corresponds to the relevance of the redox mechanism and thus allows for assessing the complexity of the actual reaction network. As illustrated in Fig. 8, the $r(CO_2)/r(C_3H_8)$ ratio for all catalysts ranges from 0.22 to 0.75, which is significantly smaller than 1.0. Furthermore, the highest stable $r(CO_2)/r(C_3H_8)$ ratio, ~ 0.75 ± 0.05 %, occurs over the 3 %Cu(Ce/Zn) sample, which is in line with its superior activity in CO_2-ODHP. This observation could be attributed to the concurrent appearance of the DHP reaction to varying degrees, as supported CuO_x also serves as an effective catalyst for the DHP reaction [38]. Considering the highest $r(CO_2)/r(C_3H_8)$ ratio and the best activity of 3 %Cu(Ce/Zn) in CO_2-ODHP, it is proposed that both C-H and C-O bonds in C_3H_8 and CO_2 atoms could be activated over CuO_x dispersed on (Ce/Zn) lattice, with the effectiveness depending on the structural properties of the Cu^{2+} oxides.

Table 3 and Fig. S7 (see SM) compare the performance data obtained for the catalysts synthesized in this study with those published in the literature. Lawson et al. found that Ga_{15}/ZSM-5 exhibited a propene yield of 25.9 % at 550 °C [39]. Furthermore, Castillón-Barraza et al. reported a higher propene yield of 39.4 % at the same temperature, though using a much more expensive noble metal-based catalyst, i.e. Pt/Sn on SBA-15, with the incorporation of MgO catalysts [40]. Although these catalysts showed better propene yields, it is important to mention that

Table 3
Comparison with catalysts in the literature for CO_2–ODHP.

Catalysts	Gas composition	T (°C)	Conversion (%)	Selectivity (%)	Yield (%)	Ref.
0 %Cu(Ce/Zn)	4 %C_3H_8/8 %CO_2/88 %Ar	550	38.76	57.03	22.10	TW
1 %Cu(Ce/Zn)	4 %C_3H_8/8 %CO_2/88 %Ar	550	43.98	54.86	24.12	TW
2 %Cu(Ce/Zn)	4 %C_3H_8/8 %CO_2/88 %Ar	550	45.08	54.39	24.52	TW
3 %Cu(Ce/Zn)	4 %C_3H_8/8 %CO_2/88 %Ar	550	46.93	53.73	25.21	TW
V-Sb-O/SiO_2	1 %C_3H_8/4 %CO_2 in N_2	600	40.10	65.60	26.30	[41]
4 %Zn/Na SSZ-39	1 %C_3H_8/1 % CO_2/18 %N_2	600	43.00	62.79	27.00	[43]
Ga_{15}/ZSM-5	1 %C_3H_8/1 % CO_2/8 %N_2	550	37.00	70.00	25.90	[39]
CrO_x/silicate-1	4 %C_3H_8/20 % CO_2/1 %A_r	550	25.00	85.00	21.25	[7]
VO_x/SiO_2	1 %C_3H_8/2 % CO_2/7 %Ar	550	25.00	45.00	11.25	[44]
5GaN/S-1	1 %C_3H_8/2 % CO_2/7 %N_2	600	23.00	91.00	20.93	[1]
Cu/Ga-MFI	3 %C_3H_8/3 % CO_2/4 %N_2	600	93.00	4.00	3.72	[45]
$Ru_1Cr_{10}O_x$/SiO_2	1 %C_3H_8/1 % CO_2/1 %N_2	500	9.00	90.00	8.10	[46]
CMg4	5 %C_3H_8/10 % CO_2/20 %N_2	550	42.80	92.00	39.37	[40]
5CrO_y/$Ce_{0.5}$Zr0.5O_2/SiO_2	1 %C_3H_8/2 % CO_2	675	38.00	77.00	29.00	[6]
5Cr/MCM-41	1 %C_3H_8/2 % CO_2	650	21.00	85.00	17.85	[15]
5 % CrO_x/SiO_2 (Acros)	1 %C_3H_8/2 % CO_2	700	53.00	64.15	34.00	[42]

Note: TW stands for the results obtained in this work. SSZ-39 refers to aluminosilicate zeolite, S-1 refers to a zeolite, MFI correlates to a zeolite, CMg is Pt/Sn on SBA-15 with incorporation of MgO, MCM-41 denotes the mesoporous silicates, SiO_2 (Acros) refers to amorphous silicas.

3 %Cu(Ce/Zn) exhibited a higher propane conversion rate of 46.9 % compared to those in the literature. At 600 °C, Zhang et al. [41] and Zhou et al. [20] reported propane yields of 26.3 % and 27.0 %, respectively. Additionally, at much higher temperatures, Mashkin et al. [6] and Tedeeva et al. [42] achieved increased yields of 29.0 % and 34.0 %, respectively. It is worth mentioning that the interplay between Cu, Ce, and Zn in the catalyst samples subject to the present study provided significant catalytic activity, making 3 %Cu(Ce/Zn) a promising candidate for industrial applications.

4. Discussion

Developing a suitable catalyst with both high activity and selectivity to the intended product is a key objective in the field of catalysis. However, since scaling correlations generally apply to complex reactions, improvements in catalytic performance often lead to various side reactions, which in turn reduce product selectivity and promote coke generation [7,20]. Therefore, understanding the structure-activity correlation is crucial for enhancing catalytic activity. As already discussed in the introduction, this is particularly relevant for supported CuO_x catalysts that are used in propane dehydrogenation processes. In the following sections, the nature of the scaling correlations will be explored for CO_2-ODHP over the Cu(Ce/Zn) catalysts, focusing on the impacts of the CuO_x structure on catalytic performance, propene selectivity, coke deposition and stability.

4.1. The structural relationship of CuO_x with the catalytic activity and selectivity

The results presented in Sections 3.4 and 3.6 reveal that the starting value of C_3H_8 or CO_2 conversion at a TOS of 20 min over Cu(Ce/Zn) catalysts appears to increase with a higher amount of Cu^{2+} oxides present in the catalysts. To verify this, the quantity of Cu^{2+} oxides in Cu(Ce/Zn) was evaluated from the H_2-TPR analysis (Fig. 4), considering that H_2 consumption correlates directly with the reducibility of Cu^{2+} to Cu^+ oxides during the incorporation of Cu into the (Ce/Zn) lattice. The corresponding findings, which relate the starting value of propane conversion at a TOS of 20 min to the amount of Cu^{2+} oxides, are depicted in Fig. 9. A strong linear relationship was observed between the initial C_3H_8 conversion and the quantity of Cu^{2+} oxides in the Cu(Ce/Zn) catalyst (Fig. 9a). This result suggests that the quantity of Cu^{2+} oxides is a crucial element in examining the performance of Cu(Ce/Zn) catalyst for CO_2-ODHP, a conclusion that aligns with findings in the literature regarding DHP and CO_2-ODHP [38,45].

As already mentioned above, the selectivity for C_3H_6 (Fig. 6c) appears to change inversely to the initial conversion of C_3H_8 (Fig. 6a). Plotting the initial C_3H_6 selectivity observed at a TOS of 20 min against the amount of Cu^{2+} of the catalyst samples investigated herein (Fig. 9b) strongly suggests that a larger quantity of Cu^{2+} on the catalyst corresponds to a lower propene selectivity. Cu-free sample exhibited the highest selectivity. According to XPS results (Fig. 3 and Table S3), this behavior could be related to its highest amount of Ce^{4+} species on the catalyst surface, which favors the desorption activity of propene and significantly enhances the propene selectivity and the coke generation during the CO_2-ODHP process [21].

Furthermore, the activity of the Cu(Ce/Zn) catalysts (Fig. 6) correlates with their SSA and pore volume (c.f. BET results, Table 1): A high SSA and pore volume, as observed with increasing Cu-loading, facilitate the mobility of active sites and O_{Lat}, playing an important role in CO_2-ODHP. XPS analysis indicated that the catalytic behavior correlates well with the generation of O_{Lat}, and the presence of increased amounts of Cu^{2+}, Ce^{3+}, and Zn^{2+} species. Additionally, the smallest crystallite size and E_g were observed for 3 %Cu(Ce/Zn), as demonstrated by XRD and UV-vis analyses, which are known to be advantageous for the CO_2-ODHP reaction as well [8,20]. Also, the performance of the Cu(Ce/Zn) samples is linked to their high inherent reducibility. This substantial reducibility could be attributed to the oxidation-reduction equilibrium of $Cu^{2+} + Ce^{3+} \leftrightarrow Cu^+ + Ce^{4+}$, as well as the synergetic effect of CeO_2 and CuO on the surface of Cu(Ce/Zn), which increased the interaction between Cu and Ce ions [25]. Furthermore, Fig. S8 (see SM) depicts the variation of the reaction rate and turnover frequencies (TOF) over TOS. The highest reaction rate and TOF were achieved by 3 %Cu(Ce/Zn). Consequently, it can be stated that the 3 %Cu(Ce/Zn) catalyst exhibits the best possible conversion of C_3H_8 and yield of C_3H_6 due to its electronic and structural properties.

4.2. Insights into catalytic stability and coke deposition

Characterization and reaction findings suggest that the Cu(Ce/Zn) catalyst with a smaller amount of Cu^{2+} oxides could experience faster deactivation because of a stronger adsorption of C_3H_6 molecules. The average deactivation rate decreases as the Cu loading increases from 1 to 3 wt.% (Fig. 7). Coke formation during the oxidative dehydrogenation process is generally related to catalyst deactivation [7]. Therefore, the spent sample after CO_2-ODHP under the parameters outlined in Fig. 6 underwent TGA analyses. As illustrated in Fig. S9 (see SM), weight loss is observed for all the catalysts, correlating to the removal of absorbed water and the combustion of deposited coke, respectively. The trend of the coke quantity relative to Cu loading over Ce/Zn (Fig. 7) in-

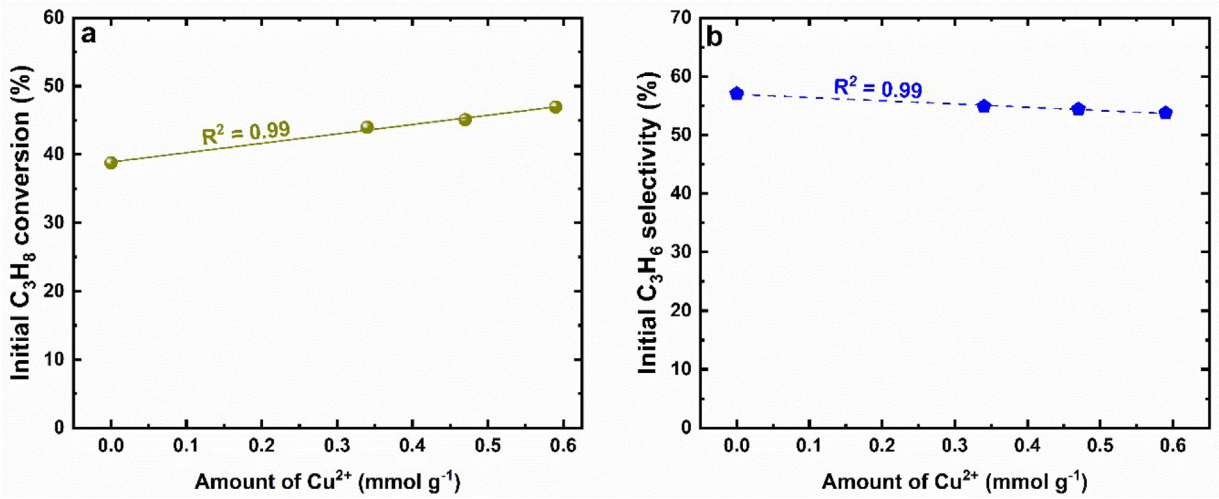

Fig. 9. The initial C_3H_8 conversion vs. the amount of Cu^{2+} oxides (a), and the correlation of the initial C_3H_6 selectivity with the amount of Cu^{2+} oxides (b) over Cu(Ce/Zn) catalysts. GHSV = 12,000 h^{-1}, and gas composition: 4 % C_3H_8, 8 % CO_2, diluted in Ar. T = 550 °C.

dicates that coke formation defavors the stability and enhances the catalyst's selectivity for CO_2-ODHP. In this study, the coke has two potential deposition sites. It primarily agglomerates on Ce^{3+}-O vacancy pairs and Cu^{2+} sites, which block CO_2 activation centers. In addition, it accumulates at the pore mouths in the (Ce/Zn) lattice, restricting propane diffusion to the active sites. In reality, the deposited coke has been shown to improve the selectivity to the desired product C_3H_6 by preferentially contaminating the most active positions responsible for unwanted side reactions, such as transalkylation, namely the carbonaceous impurities [7]. Additionally, coke obstructs access to Ce^{3+}/Ce^{4+} redox sites, which is crucial for CO_2 activation and critical for H-abstraction, ultimately reducing C_3H_8 conversion and propane turnover frequency (TOF). Furthermore, coke diminishes the availability of over-oxidation sites (Ce^{4+}-O*), hindering the combustion of propene to CO_x, and thus increasing C_3H_6 selectivity. In this study, amorphous coke was identified as the primary cause of rapid catalyst deactivation. It preferentially forms and accumulates at the most active sites, directly blocking the activation of C_3H_8 [47]. In contrast, graphitic coke has a less significant and slower impact on active sites, mainly agglomerating on the support due to its lower reactivity [47]. Moreover, the catalytic stability increases with the reduction of the coke deposited on the catalysts. This finding is in line with previous works [48]. According to Xing et al. [49], the coke can be consumed by the lattice oxygen (O_{Lat}) originating from the catalyst, especially from CeO_2 in the support, which is slightly reduced to create an oxygen vacancy. This vacancy is subsequently filled by an oxygen molecule generated from the activation of CO_2, allowing for continuous coke removal via the redox reactions of CeO_2 that are believed to follow a Mars-van Krevelen mechanism [21]. After all, this process greatly increases coke resilience and catalyst stability. The presence of CeO_2 in the catalysts was proven with XRD analysis, and based on XPS, the presence of Cu^{2+} inside the (CeZn) structure considerably increased the amount of O_{Lat}. That the 3 %Cu(Ce/Zn) sample exhibits the highest amount of O_{Lat} matches well with the performance data, as this is the catalyst sample with the best stability (Fig. 7).

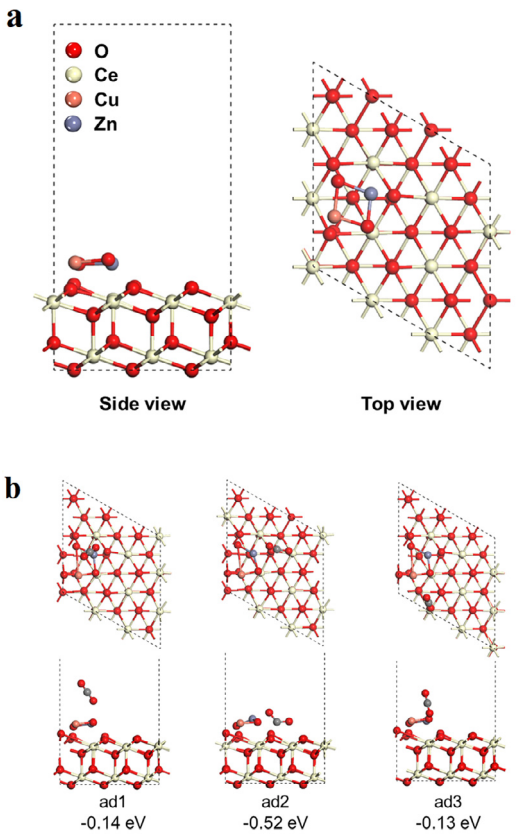

Fig. 10. Structure of CeO_2-supported CuO-ZnO periodic surface model (a), and the adsorption energy of CO_2 on different sites of the CeO_2-supported CuO-ZnO surfacemodel (b).

4.3. Adosorption energes of CO_2 on the CeO_2/CuO/ZnO surface

The established CeO_2-supported CuO-ZnO periodic surface model is shown in Fig. 10a. A six-layer CeO_2 (111) surface slab is cleaved from the perfect CeO_2 (111) crystal, with each Ce layer sandwiched between two oxygen layers. A CuO-ZnO catalytic cluster is anchored on the CeO_2 (111) surface, positioning its Cu and Zn atoms adjacent to the coordinately unsaturated O sites. Three CO_2 adsorption structures are identified, including CO_2 over the top site of the CuO-ZnO cluster, the unsaturated O top site of the CeO_2 surface, and an interference site between the surface and the CuO-ZnO cluster, as illustrated in Fig. 10b. The adsorption energies on the CuO-ZnO top site and the unsaturated O top site of the CeO_2 (111) surface are −0.14 eV and −0.13 eV, respectively, with no significant torsion of CO_2 observed after adsorption, indicating physical adsorption. In contrast to the adsorption site at the interface between CeO_2 and the CuO-ZnO cluster, the adsorption energy is −0.52

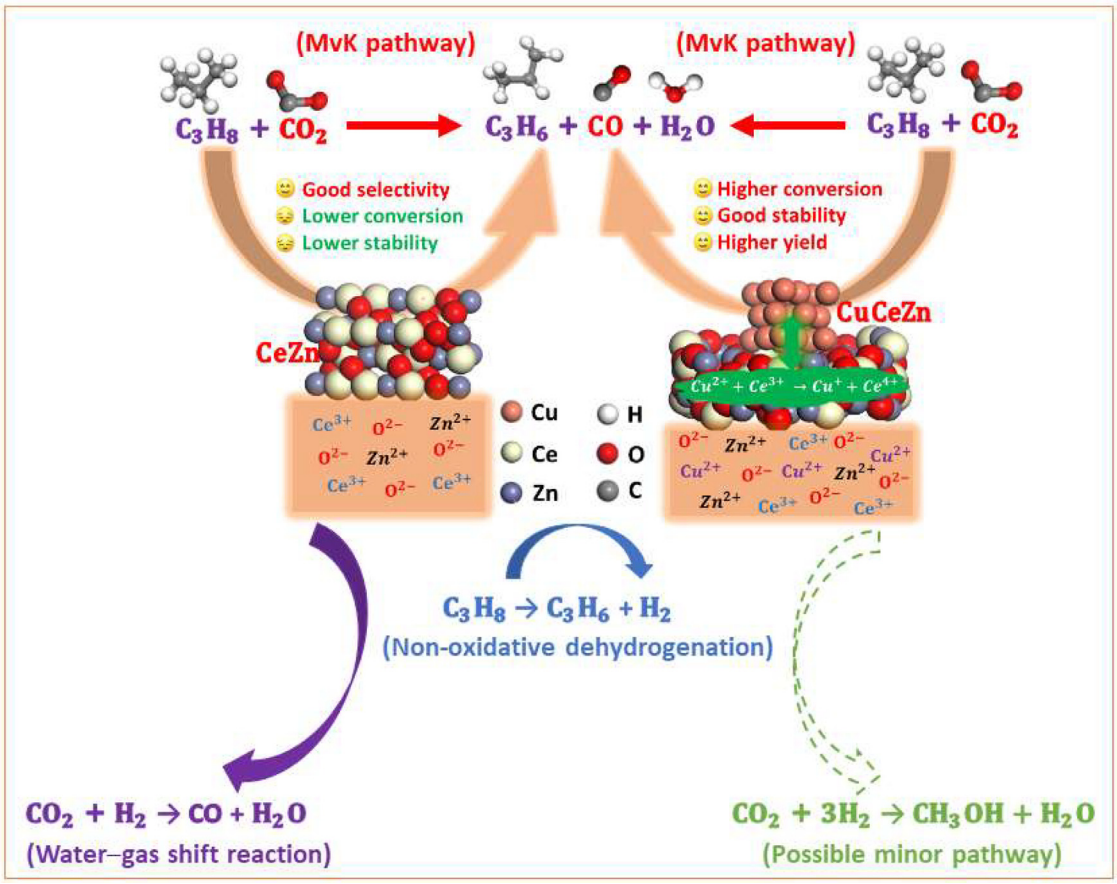

Scheme 1. Proposed reaction pathways for CO_2–ODHP over Cu(Ce/Zn) catalysts, highlighting the interplay between oxidative and non-oxidative routes.

eV, and the O–C-O angle is 127° after adsorption, which corresponds to chemical adsorption. Therefore, the CuO-ZnO cluster on the CeO_2 (111) surface effectively promotes the activation of CO_2.

4.4. Active and selective nature of Cu(Ce/Zn) for CO_2-ODHP

Taking into account the findings and discussions stated above, Scheme 1 illustrates the mechanistic possibilities for CO_2-ODHP over Cu(Ce/Zn) catalysts. In the oxidative route, propane undergoes C-H activation on Cu^{2+} oxide sites, with lattice oxygen or activated CO_2 species participating in a Mars-van Krevelen type mechanism to produce propene and surface hydroxyls. In parallel, a non-oxidative dehydrogenation route may operate, where propane is directly dehydrogenated to propene and H_2 without lattice oxygen involvement. The generated H_2 can further react with CO_2 via the water–gas shift (WGS) reaction, producing CO and H_2O. In addition, given the established reactivity of CuO–ZnO systems, the hydrogenation of CO_2 to methanol represents a potential side reaction, although no significant methanol was detected in this study. The balance between these oxidative and non-oxidative processes, along with coke deposition dynamics, governs the observed activity, selectivity, and stability trends for Cu(Ce/Zn) catalysts. A single atom of a propane molecule is firmly adsorbed on the most active Cu^{2+} oxides, which facilitate C-H bond activation and increase the initial conversion rate through Cu incorporation inside the (Ce/Zn) structure. However, the desorption of the produced propene molecules from these sites can be hindered, resulting in increased secondary reactions such as cracking and coke deposition, which ultimately reduces propene selectivity. With time-on-stream, the most active Cu^{2+} oxides become progressively covered by the deposited coke. Concurrently, fewer atoms of the propane molecule are adsorbed onto the Cu^{2+} oxides. As a result, C_3H_8 conversion steadily decreases, whereas C_3H_6 selectivity gradually increases. This shift depends on the amount of specific Cu^{2+} oxides present on the Cu(Ce/Zn) catalyst. Once the majority of active Cu^{2+} oxide sites are nearly completely enveloped by the deposited coke, the near-constant propane conversion and propene selectivity are achieved, and the reaction rates are stable. Hence, the various quantities of the Cu^{2+} oxides, which are governed by the Cu loadings over (Ce/Zn) lattice, account for the differences in propane conversion and propene selectivity over TOS for CO_2-ODHP.

While the above discussion assumes a Mars–van Krevelen type mechanism involving CO_2 activation and subsequent oxidative dehydrogenation, alternative pathways should also be considered. One possibility is catalytic (non-oxidative) dehydrogenation of propane, in which direct C–H activation produces propene and H_2 without lattice oxygen participation. In this scenario, the generated H_2 could further participate in the water–gas shift (WGS) reaction with CO_2, producing CO and H_2O. Furthermore, given the well-established activity of CuO–ZnO materials for CO_2 hydrogenation to methanol, the formation of H_2 from non-oxidative dehydrogenation raises the possibility of methanol as a minor by-product under reaction conditions. Although no significant methanol was detected in the present study, its potential formation pathway cannot be excluded and merits further mechanistic investigation. Thus, the overall catalytic performance of Cu(Ce/Zn) in CO_2-ODHP likely arises from a complex interplay of oxidative and non-oxidative routes, with CO_2 playing dual roles as both a mild oxidant and a reactant in side processes such as WGS or methanol synthesis. Future studies involving in situ spectroscopic techniques and isotopic labeling will be crucial to unambiguously delineate the contributions of these parallel pathways.

Furthermore, the roles of Cu, Ce, and Zn were closely interconnected during the CO_2-ODHP reaction. First, Ce served as the main driver of the catalytic activity through the Ce^{3+}/Ce^{4+} redox cycling, as confirmed by

XPS and H_2-TPR analyses. Second, Cu modulated the Ce^{3+}/Ce^{4+} cycle instead of predominantly transitioning between Cu^{2+}/Cu^{+}. The stabilization of oxygen vacancies by the presence of Cu enhanced the electron transfer between Ce and propane, which accelerated the dehydrogenation process and improved the effectiveness of CO_2 activation. Lastly, Zn acted as a structural promoter that stabilized the catalyst lattice, preventing sintering and ensuring the dispersion of active sites. Regarding the native oxygen species (O*), the reactive O* originated from the lattice oxygen (O_{Lat}) within the (CeZn) framework, as reported in previous studies [21]. The O_{Lat} became mobile when Ce^{4+} was reduced to Ce^{3+}, and CO_2 dissociation on Ce^{4+} produced CO and lattice O* [21]. Based on those mentioned above, a reaction mechanism is proposed and described in Eqs. (17)-(24):

• **Step 1:** During CO_2 activation, CO_2 adsorbs onto Ce^{4+}, reducing it to Ce^{3+} while releasing lattice O*. In this process, Cu plays a crucial role by lowering the energy barrier for the reduction of Ce^{4+} and stabilizing the O* intermediates.

$$Ce^{4+} + CO_2 \; Ce^{3+} + CO + O*_{(lattice)} \tag{17}$$

$$Cu\; Ce^{3+}/Ce^{4+}(electron\; transfer\;\; \mathrm{mod}\, ulation) \tag{18}$$

$$Zn\; Ce^{4+}(lattice\; stabilization\; and\; surface\; optimization) \tag{19}$$

• **Step 2:** In propane dehydrogenation, O* abstracts hydrogen from propane, resulting in the formation of propene and water

$$C_3H_8 + O* \;\; C_3H_6 + H_2O \tag{20}$$

• **Step 3:** In the redox cycle regeneration, Ce^{3+} is reoxidized by O_2 or residual CO_2, which restores the active Ce^{4+} sites.

$$Ce^{3+} + O_2 \; Ce^{4+} + 2\; O* \tag{21}$$

Alternatively,

• **Step 4:** Non-oxidative dehydrogenation can occur, producing byproduct H_2, particularly when the availability of lattice O* is limited.

$$C_3H_8 \; C_3H_6 + H_2 \tag{22}$$

• **Step 5:** Water gas shift reaction can occur in parallel, impacting the equilibrium of $H_2/CO/CO_2$ and potentially influencing the selectivity for propene.

$$CO_2 + H_2 \; CO + H_2O \tag{23}$$

• **Step 6:** A possible minor pathway could involve the formation of methanol. However, no methanol was detected during the experiment.

$$CO_2 + 3H_2 \; CH_3OH + H_2O \tag{24}$$

5. Conclusion

In summary, a series of Cu(Ce/Zn) catalysts with well-defined structures and CuO_x species compositions were synthesized by impregnating up to 3 wt.% Cu onto (CeZn) for CO_2-ODHP at 550 °C. The structural and chemical characteristics of the different Cu(Ce/Zn) catalysts were analyzed in a comprehensive manner and then correlated to the catalytic performance data, i.e. propane conversion and propene selectivity. During activity tests, a 3 wt.% Cu loading in (CeZn) lattice was found to enable the highest C_3H_6 yield of 25.2 %. Characterization results uncover the presence of Cu^{2+} oxides in all Cu(Ce/Zn) catalysts, with their quantities increasing with increasing Cu loadings. The correlation between catalyst performance and characterization revealed that Cu^{2+} oxides are more active but not as selective as the Ce^{4+} oxides in CO_2-ODHP, promoting the advantageous activation of propane molecules to form radicals and enhancing subsequent reactions of the generated propene due to strong adsorption. Additionally, the formed and accumulated coke on the catalyst serves dual roles by lowering C_3H_8 conversion while increasing C_3H_6 selectivity. These findings clarify the observed initial C_3H_6 yields, which increase in the order of 0 %Cu(Ce/Zn) < 1 %Cu(Ce/Zn) < 2 %Cu(Ce/Zn) < 3 %Cu(Ce/Zn), and the stability, which decreases in the same order. Hence, loading Cu into the (Ce/Zn) structure was found to promote the catalytic activity with CO_2. Moreover, DFT calculations demonstrated that CuO-ZnO cluster on the CeO_2 (111) surface efficiently enhances the activation of CO_2. The obtained results reveal the optimum loading of copper into (Ce/Zn) as an efficient catalyst for CO_2-ODHP. Further investigations could enhance the fundamental mechanistic understanding of the structure-activity dualism and the relationships among the Cu, Ce, and Zn. For instance, a comprehensive understanding of the formation of oxygen vacancy sites and F^{+} centers could be investigated by an electron paramagnetic resonance (EPR) at room temperature (297 K). Additionally, post-reaction Cu particle size characterization would provide valuable insight into the deactivation mechanism, particularly regarding potential sintering, and increasing Cu loading beyond 3 wt.% would determine the optimal loading and its effect on catalyst performance. However, the novel catalyst materials proposed herein exhibit significant potential for application in the petrochemical industry.

Data availability

All the relevant data are available from the authors upon request.

Declaration of competing interest

The authors declare that they have no conflicts of interest in this work.

CRediT authorship contribution statement

Cedric Karel Fonzeu Monguen: Writing – original draft, Investigation, Formal analysis. **Samuel Daniel:** Writing – review & editing, Investigation. **Ling-Nan Wu:** Formal analysis. **Hannington Nevin Otieno:** Investigation. **Patrick Lott:** Writing – review & editing, Methodology. **Wu Qin:** Validation, Software. **Olaf Deutschmann:** Writing – review & editing, Supervision. **Zhen-Yu Tian:** Writing – review & editing, Validation, Supervision, Funding acquisition, Conceptualization.

Acknowledgments

This work was financially supported by the National Natural Science Foundation of China (52325604/W2412101), Ministry of Science and Technology of China (2021YFA0716200/2022YFB4003900), and the Helmholtz Association (Germany) within the Helmholtz-Program MTET: Materials and Technologies for the Energy Transition. We are also grateful for the financial support from the ANSO scholarship. We finally thank A. Knapp (Institute for Chemical Technology and Polymer Chemistry, Karlsruhe Institute of Technology, Germany) for the TGA analysis.

Supplementary materials

Supplementary material associated with this article can be found, in the online version, at doi:10.1016/j.fmre.2025.11.006.

References

[1] Z.-J. Zhu, Z.-H. He, Y. Tian, et al., Mass-transfer enhancement in the CO_2 oxidative dehydrogenation of propane over GaN supported on zeolite nanosheets with ashort b-axis and hierarchical pores, ACS Catal 14 (2024) 10376–10391.
[2] Y. Gambo, S. Adamu, A.A. Abdulrasheed, et al., Catalyst design and tuning for oxidative dehydrogenation of propane – A review, Appl. Catal. A. Gen. 609 (2021) 117914.

[3] C.K. Fonzeu Monguen, A. El Kasmi, M.F. Arshad, et al., Oxidative dehydrogenation of propane into propene over chromium oxides, Ind. Eng. Chem. Res. 61 (2022) 4546–4560.
[4] S. Daniel, C.K. Fonzeu Monguen, L. Wu, et al., Flame synthesis of Zr/ZSM-5 catalysts with tunable acidity for the oxidative dehydrogenation of propane to propene, J. Thermal Sci. 33 (2024) 268–283.
[5] X. Jiang, L. Sharma, V. Fung, et al., Oxidative dehydrogenation of propane to propylene with soft oxidants via heterogeneous catalysis, ACS Catal. 11 (2021) 2182–2234.
[6] M.Y. Mashkin, M.A. Tedeeva, A.A. Fedorova, et al., Synthesis of $Ce_xZr_{1-x}O_2/SiO_2$ supports for chromium oxide catalysts of oxidative dehydrogenation of propane with carbon dioxide, J. Chem. Technol. Biotechnol. 98 (2023) 1247–1259.
[7] J. Wang, Y.-H. Song, Z.-T. Liu, et al., Active and selective nature of supported CrO_x for the oxidative dehydrogenation of propane with carbon dioxide, Appl. Catal. B. Environ. 297 (2021) 120400.
[8] Z.-Y. Wang, Z.-H. He, Y. Xia, et al., Oxidative dehydrogenation of propane to propylene in the presence of CO_2 over gallium nitride supported on NaZSM-5, Ind. Eng. Chem. Res. 60 (2021) 2807–2817.
[9] J. Liu, N. He, Z. Zhang, et al., Highly-dispersed zinc species on zeolites for the continuous and selective dehydrogenation of ethane with CO_2 as a soft oxidant, ACS Catal. 11 (2021) 2819–2830.
[10] S. Song, K. Yang, P. Zhang, et al., Silicalite-1 stabilizes Zn-hydride species for efficient propane dehydrogenation, ACS Catal. 12 (2022) 5997–6006.
[11] Z.Y. Wang, Z.H. He, L.Y. Li, et al., Research progress of CO2 oxidative dehydrogenation of propane to propylene over Cr-free metal catalysts, Rare Metals 41 (2022) 2129–2152.
[12] R.X. Valenzuela, G. Bueno, V. Cortés Corberán, et al., Selective oxidehydrogenation of ethane with CO_2 over CeO_2-based catalysts, Catal. Today 61 (2000) 43–48.
[13] A. El Kasmi, M.F. Arshad, M. Waqas, et al., Insights into catalytic oxidation mechanism of CO over Cu catalyst: experimental and modeling study, Mater. Res. Bull. 166 (2023) 112343.
[14] C.K.F. Monguen, S. Daniel, Z.-Y. Tian, Controlled synthesis of Cu-Cr double-layer thin films for oxidative dehydrogenation of propane at low temperature, Chem. Eng. J. 474 (2023) 145769.
[15] M. Igonina, M. Tedeeva, K. Kalmykov, et al., Properties of CrO_x/MCM-41 and its catalytic activity in the reaction of propane dehydrogenation in the presence of CO_2, Catalysts 13 (2023) 906.
[16] B. Qiu, W.-D. Lu, X.-Q. Gao, et al., Borosilicate zeolite enriched in defect boron sites boosting the low-temperature oxidative dehydrogenation of propane, J. Catal. 408 (2022) 133–141.
[17] B. Delley, From molecules to solids with the $DMol^3$ approach, J. Chem. Phys. 113 (2000) 7756–7764.
[18] J.P. Perdew, K. Burke, M. Ernzerhof, Generalized gradient approximation made simple, Phys. Rev. Lett. 77 (1996) 3865–3868.
[19] R.D. Shannon, Revised effective ionic radii and systematic studies of interatomic distances in halides and chalcogenides, Acta Crys. 32 (1976) 751–767.
[20] S. Zhou, H. Zhang, X. Jiang, et al., CO_2-mediated oxidative dehydrogenation of propane over Zn modified SSZ-39 catalysts, ChemCatChem. 16 (2024) e202400939.
[21] S. Daniel, C.K. Fonzeu Monguen, Z.-Y. Tian, Unraveling the influence of CO_2 and Ce loading over ZSM-5 for oxidative dehydrogenation of propane, Chem. Eng. J. 485 (2024) 150009.
[22] H. Dai, A. Zhang, R. Wang, et al., Investigation of different ratio of CuCe catalysts applied in photothermal reverse water gas shift reaction, Appl. Catal. A. Gen. 686 (2024) 119927.
[23] R. Ye, L. Ma, J. Mao, et al., A Ce-CuZn catalyst with abundant Cu/Zn-O_V-Ce active sites for CO_2 hydrogenation to methanol, Nature Commun. 15 (2024) 2159.
[24] B. Yang, W. Deng, L. Guo, et al., Copper-ceria solid solution with improved catalytic activity for hydrogenation of CO_2 to CH_3OH, Chinese J. Catal. 41 (2020) 1348–1359.
[25] C.K. Fonzeu Monguen, S. Daniel, Z.-Y. Tian, Low-temperature deep oxidation of N,N-dimethylformamide (DMF) over CeCu binary oxides, Catal. Sci. Technol. 13 (2023) 3517–3526.
[26] X. Zheng, Y. Li, L. Zhang, et al., Insight into the effect of morphology on catalytic performance of porous CeO_2 nanocrystals for H_2S selective oxidation, Appl. Catal. B. Environ. 252 (2019) 98–110.
[27] O. Elmutasim, A.G. Hussien, A. Sharan, et al., Evolution of oxygen vacancy sites in ceria-based high-entropy oxides and their role in N_2 activation, ACS Appl. Mater. Interf. 16 (2024) 23038–23053.
[28] R.M. Rakhmatullin, V.V. Semashko, S.L. Korableva, et al., EPR study of ceria nanoparticles containing different concentration of Ce^{3+} ions, Mater. Chem. Phys. 219 (2018) 251–257.
[29] F. Ma, X. Liu, X. Wang, et al., Atomically dispersed Zn-Co-N-C catalyst boosting efficient and robust oxygen reduction catalysis in acid via stabilizing Co-N bonds, Fundam. Res. 3 (2023) 909–917.
[30] C.K.F. Monguen, A.E. Kasmi, S. Daniel, et al., Structure sensitivity of propane partial oxidation over chromium-manganese binary oxides, Proc. Comb. Inst. 39 (2023) 5657–5666.
[31] C.K. Fonzeu Monguen, E.-J. Ding, S. Daniel, et al., Tailored synthesis of catalytically active cerium oxide for N, N-dimethylformamide oxidation, Mater 16 (2023) 865.
[32] G. Umadevi, K.G. Krishna, V.D. Mote, Green synthesis of $ZnCeO_2$ and $ZnCuCeO_2$ nanocomposites for enhanced gas sensing: a synergistic approach towards sustainable ammonia detection, J. Mater. Sci. Mater. Electronics. 35 (2024) 1511.
[33] M.B. Ansari, S.-E. Park, Carbon dioxide utilization as a soft oxidant and promoter in catalysis, Energy Environ. Sci. 5 (2012) 9419–9437.
[34] X. Li, J. Feng, Z. Xu, et al., Cerium modification for improving the performance of Cu-SSZ-13 in selective catalytic reduction of NO by NH_3, React. Kin. Mechan. Catal. 128 (2019) 163–174.
[35] S. Bepari, M. Khan, X. Li, et al., Effect of Ce and Zn on Cu-based mesoporous carbon catalyst for methanol steam reforming, Topics Catal. 66 (2023) 375–392.
[36] T.R. Reina, S. Ivanova, O.H. Laguna, et al., WGS and CO-PrOx reactions using gold promoted copper-ceria catalysts: bulk CuOCeO2 vs. CuOCeO2/Al2O3 with low mixed oxide content, Appl. Catal. B. Environ. 197 (2016) 62–72.
[37] J.E. Morales-Mendoza, F. Paraguay-Delgado, Widening UV–Vis absorption band by Cu doped ZnO and ZnO/CuO composite, Mater. Lett. 291 (2021) 129494.
[38] S. Sun, M. Zhao, H. Liu, et al., Photothermal oxidative dehydrogenation of propane to propylene over Cu/BN catalysts, Front. Chem. 12 (2024) 1439185.
[39] S. Lawson, A. Farsad, B. Adebayo, et al., A novel method of 3D printing high-loaded oxide/H-ZSM-5 catalyst monoliths for carbon dioxide reduction in tandem with propane dehydrogenation, Adv. Sust. Syst. 5 (2021) 2000257.
[40] F.F. Castillón-Barraza, A. Sólis-Garcia, S.A. Gómez, et al., Propane CO_2-oxidative dehydrogenation catalyzed by Pt-Sn supported on magnesium-chemically grafted SBA-15, Mol. Catal. 565 (2024) 114384.
[41] H. Zhang, S. Cao, Y. Zou, et al., Highly efficient V–Sb–O/SiO_2 catalyst with Sb atom-isolated VOx species for oxidative dehydrogenation of propane to propene, Catal. Commun. 45 (2014) 158–161.
[42] M.A. Tedeeva, A.L. Kustov, P.V. Pribytkov, et al., Dehydrogenation of propane with CO_2 on supported CrOx/SiO_2 catalysts, Russian J. Phys. Chem. A. 92 (2018) 2403–2407.
[43] S. Zhou, H. Zhang, X. Jiang, et al., CO2-mediated oxidative dehydrogenation of propane over Zn modified SSZ-39 catalysts, ChemCatChem. n/a (2024) e202400939.
[44] J. Kang, A.D. Czaja, V.V. Guliants, Carbon dioxide as feedstock in selective oxidation of propane, European J. Inorg. Chem. 2017 (2017) 4757–4762.
[45] K. Bu, Y. Kang, Y. Li, et al., CO_2-assisted propane dehydrogenation to aromatics over copper modified Ga-MFI catalysts, Appl. Catal. B. Environ. 343 (2024) 123528.
[46] R. Jin, J. Easa, D.T. Tran, et al., Ru-promoted CO_2 activation for oxidative dehydrogenation of propane over chromium oxide catalyst, Catal. Sci. Technol. 10 (2020) 1769–1777.
[47] M. Filez, P. Walke, H. Le-The, et al., Nanoscale chemical diversity of coke deposits on nanoprinted metal catalysts visualized by tip-enhanced raman spectroscopy, Adv. Mater. 36 (2024) 2305984.
[48] Y. Yuan, W.N. Porter, J.G. Chen, Comparison of direct and CO_2-oxidative dehydrogenation of propane, Trends Chem. 5 (2023) 840–852.
[49] F. Xing, Y. Nakaya, S. Yasumura, et al., Ternary platinum–cobalt–indium nanoalloy on ceria as a highly efficient catalyst for the oxidative dehydrogenation of propane using CO_2, Nature Catal. 5 (2022) 55–65.

Author profile

Cedric Karel Fonzeu Monguen received his PhD in Power Engineering and Engineering Thermophysics from the University of Chinese Academy of Sciences (UCAS) in June 2023 under the supervision of Prof. Zhen-Yu Tian. In August 2023, he joined Karlsruhe Institute of Technology (KIT) as a senior scientist, working under the guidance of Prof. Olaf Deutschmann. His main areas of research interest are heterogeneous catalysis, hydrogen production, materials synthesis, carbon capture and environmental chemistry. The current project is the non-catalytic pyrolysis of plastic wastes for CO_2-free hydrogen production.

Zhen-Yu Tian (BRID: 03306.00.18368) got his PhD at the University of Science and Technology of China in 2008. Then he did a postdoc at CNRS in France (2008–2010) and worked at Bielefeld University as an Alexander von Humboldt Fellow and group leader (2010–2013). From August 2013, he works as a full Professor at the Institute of Engineering Thermophysics, Chinese Academy of Sciences (CAS). Tian's group mainly focuses on the combustion kinetics of engines, thin films, heterogeneous catalysis, environmental chemistry, variable gravity combustion and physical chemistry. The current project is the reaction kinetics of efficient, clean and low-carbon combustion.